Russian Chemical Reviews **84** (10) 1021 – 1050 (2015) © 2015 Russian Academy of Sciences and Turpion Ltd

DOI 10.1070/RCR4538

Qualitative and quantitative analysis of environmental samples by laser-induced breakdown spectrometry

N B Zorov, A M Popov, S M Zaytsev, T A Labutin

Department of Chemistry, Lomonosov Moscow State University
Leninskie Gory 1, str. 3, 119991 Moscow, Russian Federation

The key achievements in the determination of trace amounts of components in environmental samples (soils, ores, natural waters, *etc*.) by laser-induced breakdown spectrometry are considered. Unique capabilities of this method make it suitable for rapid analysis of metals and alloys, glasses, polymers, objects of cultural heritage, archaeological and various environmental samples. The key advantages of the method that account for its high efficiency are demonstrated, in particular, a small amount of analyzed material, the absence of sample preparation, the possibility of local and remote analysis of either one or several elements. The use of chemometrics in laser-induced breakdown spectrometry for qualitative sample classification is described in detail. Various approaches to improving the figures of merit of quantitative analysis of environmental samples are discussed. The achieved limits of detection for most elements in geochemical samples are critically evaluated.
The bibliography includes 302 references.

Contents

I. Introduction 1021
II. Fundamentals of laser-induced breakdown spectrometry and the instrumentation used 1024
III. Qualitative analysis 1027
IV. Quantitative analysis 1033
V. Conclusion 1045

I. Introduction

The last 20 years witnessed a sharp growth of the number of publications devoted to application of laser-induced breakdown spectrometry (LIBS) [1] for analysis of various samples. LIBS uses a laser ablation process when a pulsed laser generates a plasma that vaporises a small amount of a solid, gaseous or liquid sample. The emission spectrum of the excited species (as a rule, atoms) in the laser-induced plasma serves for qualitative or quantitative analysis of the sample.

N B Zorov Doctor of Chemical Sciences, Professor, Head of the Laboratory of Laser Diagnostics at the Department of Chemistry, MSU.
Telephone: +7(495)939 – 3635, e-mail: zorov@laser.chem.msu.ru
A M Popov Candidate of Chemical Sciences, Senior Researcher of the same Laboratory.
Telephone: +7(495)939 – 3635, e-mail: popov@laser.chem.msu.ru
S M Zaytsev Post-graduate student of the Department of Chemistry, MSU.
Telephone: +7(495)939 – 3635, e-mail: sergz@laser.chem.msu.ru
T A Labutin Candidate of Chemical Sciences, Senior Researcher of the same Laboratory.
Telephone: +7(495)939 – 3635, e-mail: timurla@laser.chem.msu.ru
Current research interests of the authors: spectroscopic methods of analysis, analytical laser spectrometry, analysis of multivariate data.

Received 12 November 2014
Uspekhi Khimii **84** (10) 1021 – 1050 (2015); translated by Z P Svitanko

The frequency of occurrence in the scientific literature of terms designating the laser-induced breakdown spectrometry methods and widely used analytical methods such as laser ablation inductively coupled plasma atomic emission spectroscopy (LA – ICP – AES) and laser ablation inductively coupled plasma mass spectrometry (LA – ICP – MS) according to the Google Books Ngram Viewer data (https://books.google.com/ngrams/) shows that the latter predominated starting from 1997 (Fig. 1). The gap increased with time and became really significant by the 21st century but starting from 2004, the interest in the LIBS has sharply increased, which is apparently related to its extended application in analysis.

Indeed, LIBS started to be used for determining the elemental composition of environmental samples such as minerals and rocks,[2] for sample classification [3] and for rapid real time *in situ* analysis.[4] In recent years, LIBS has proved to be efficient for the control of fake gemstones and minerals [5 – 7] that can be reliably identified and classified based on the spectral 'fingerprints' and their authenticity and provenance can be revealed. According to the data of the Materialytics company (US), which practices the determination of the provenance of minerals, the accuracy of LIBS identification is 95% for diamond and 98% for ruby and emerald. For on-line quality control of the mined mineral raw materials on the conveyor belt and at the entrance of the mining processing plant, a LIBS analyzer 'Maya' has been developed (Fig. 2). Currently, it is used, for

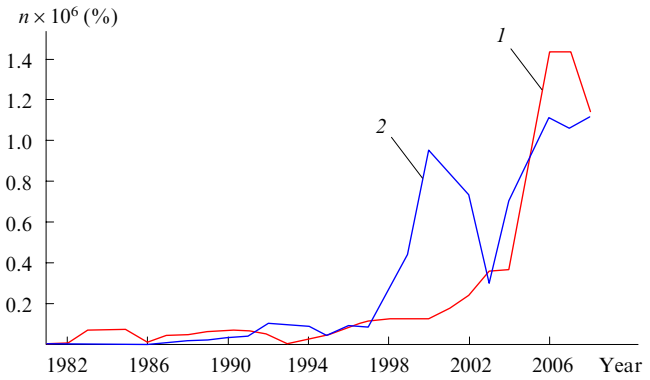


Figure 1. Frequency of occurrence (n) of terms designating LIBS methods (*1*) and the sum of LA–ICP–AES and LA–ICP–MS methods (*2*) in the publications indexed in Google Books Ngram. The vertical axis shows the number of mentions of the methods in relation to the total number of indexed words.

example, to analyze phosphate rock and coal on the moving conveyer belt [8] and in the raw magnesite screening system in the crushing line of the Magnezit crushing and beneficiation plant (Russia).[9] This device is also installed in the iron ore agglomeration unit at the Krivoi Rog iron ore plant for on-line determination of the contents of Fe, SiO_2 and CaO in the ore, ore concentrate and slime. Examples of using on-line LIBS analyzers in mining plants are presented in the publication of Gaft *et al.*[10]

Fluorine was detected in Martian rocks based on the molecular bands of calcium fluorides in the LIBS spectra by means of LIBS.[11] The LIBS technique was also used for quantitative determination of some nonmetals — sulfur in mineral raw materials,[12] carbon in soils,[13] arsenic in mine tailings [14] and even silicon in potatoes.[15] An interesting application of this method is trace analysis of individual fluid inclusions in minerals; in this case, the spatial resolution was 6–10 μm and the weight of the inclusions was $<10^{-9}$ g (Ref. 16). Laser-induced breakdown spectrometry is considered as an alternative to electron microscopy applicable in the field [17] for preliminary examination of the mineral and rock surface and structure.

A protocol and instrumentation for analysis of samples located under a water layer at a pressure of up to 30 MPa have been developed;[18,19] this makes it possible to perform measurements on the bottom of a river, lake or sea (up to 3000 m deep).[20] Successful *in situ* determinations of the composition of solid samples at a 1000 m depth [21,22] (Fig. 3) and underwater garbage in the nuclear reactor core [23] were reported. Quite a number of publications are devoted to analysis of extraterrestrial samples. First of all, this is semiquantitative analysis of samples on the Martian surface by means of the ChemCam instrument installed on the Curiosity rover (Fig. 4):[24,25] the compositions of dust, sand and various soil samples in the vicinity of the Gale crater on Mars were determined.[26,27] Calibration-free analysis of geological samples was tested on the Earth in an artificially created Martian atmosphere.[28,29]

Quite a number of monographs published in the last 10 years state the key principles, new hardware and procedures and analytical applications of LIBS. The monograph of Cremers and Radziemski mentioned above [1] is one of the first books dealing with LIBS that have attracted attention of analytical chemists. Later, there appeared a book of much larger size edited by Miziolek, Palleschi and Schechter.[30] The technical advances of the method and studies in laser plasma physics were described there in detail. New applications of the method for solving analytical problems, including applications for biomedical research, for analysis of pharmaceutical products, cultural heritage objects and so on were considered. At about the same time, the monograph edited by Singh and Thakur [31] was published. Apart from the fundamentals of LIBS, the book addressed microanalysis with high resolution both across the surface and in the depth. Considerable attention



Figure 2. Photograph of the LIBS analyzer 'Maya' above the moving conveyer belt carrying geochemical samples.
The photograph is the courtesy of M Gaft (Laser Distance Spectrometry Ltd., Israel).

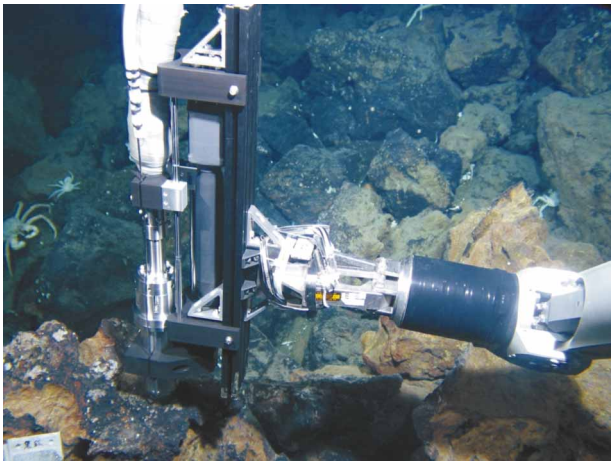


Figure 3. Underwater LIBS analyzer (ChemiCam) for multi-element determination of the composition of solid samples at a 1000 m depth in the vicinity of the Okinawa island (Japan) (http://ocean.iis.u-tokyo.ac.jp/research/laser_induced.html).

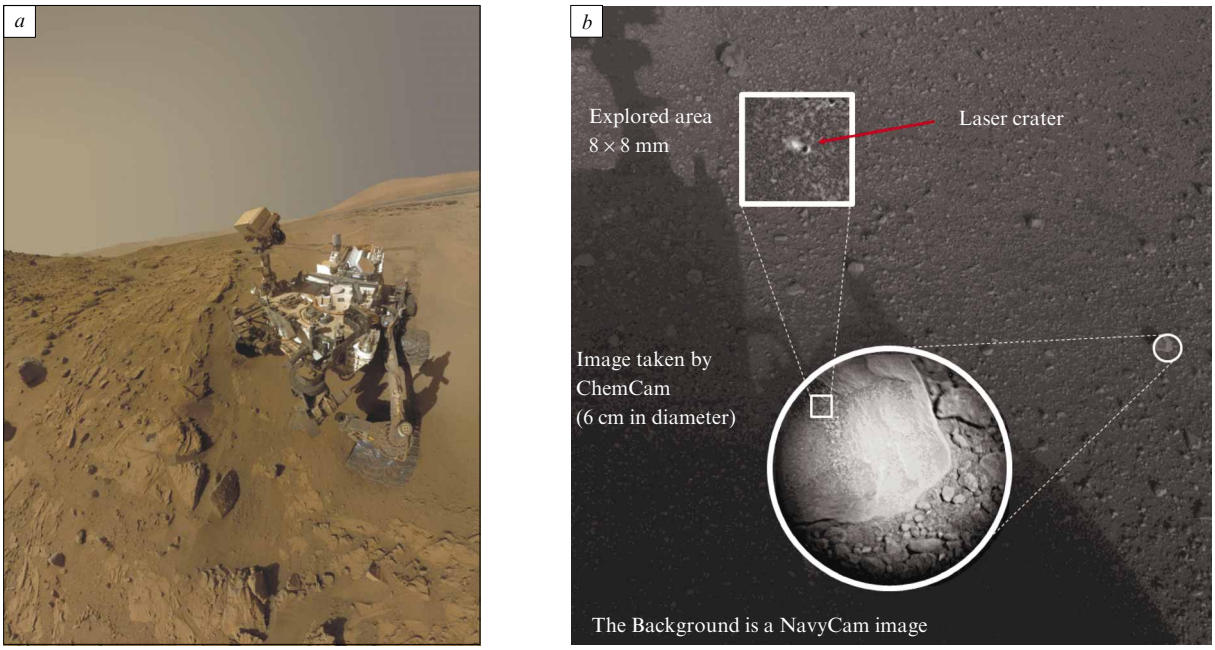


Figure 4. 'Selfie' of the Mars rover (*a*) and a Martian surface image taken by the navigation camera of the Mars rover (*b*). The circle on the right (6 cm in diameter) shows the image before the first laser shot, August 21, 2012; the larger circle shows the same enlarged image; the square (8 mm side) contains more enlarged image of the surface after the laser shot and LIBS analysis (a laser crater can be seen on the rock sample surface) (courtesy of NASA/JPL-Caltech/MSSS).

is given to analytical applications of the method, in particular, for diagnosis of combustion processes, investigation of inclusions in minerals and analysis of aerosols. The prospects for the use of LIBS and the expedients that enhance the method sensitivity and precision are stated in the chapter written by Russian researchers in the book [32] edited by Hemsworth. Noll's monograph [33] is a comprehensive source covering the physical fundamentals of the method, parameters of main processes and components of instrumentation. Of particular note is the chapter devoted to the application of LIBS in industry. Seven years after the publication of the first edition of the monograph,[1] the second, augmented edition [34] was published, which was supplemented by chapters on calibration-free LIBS and the use of chemometrics for retrieving useful information from spectral data.

A considerable number of recent reviews are devoted to fundamentals and various applications of LIBS. The review of Song *et al.*,[35] describing the prospects for the use of LIBS and instrumentation required for the design of portable LIBS devices, double-pulse LIBS, resonance ablation combined with laser-induced fluorescence should be mentioned. The guidelines for selecting experimental conditions that would ensure the best repeatability of the results and the figures of merit of LIBS were presented by Tognoni *et al.*[36] The prospects for LIBS application for exploration of archaeological findings and other cultural heritage objects constitute the subject of a paper written by Giakoumaki *et al.*[37] The key trends in the development of LIBS are described in a voluminous (almost 150 pages) review [38] of Brazilian researchers. The figures-of-merit aspects in the semiquantitative and quantitative analysis are covered in a paper of Fantoni *et al.*[39]

The review of Cremers and Chinni [40] focuses on the new applications of LIBS that have appeared in the last decade and are inaccessible for other analytical methods and outlines the limitations of LIBS. The paper of Popov *et al.*[41] is devoted to the use of LIBS for analysis of construction materials and environmental samples. The approaches employed to enhance the sensitivity of analytical measurements are compared. The development of portable LIBS instruments and those to be used in the field are covered in the review of Fortes and Laserna.[42] Italian scientists [43] reported new results on the use of LIBS-based sensors in environmental and space research and in the studies of cultural heritage objects. Two fundamental reviews of Hahn and Omenetto [44, 45] state the theoretical grounds of the method and its numerous applications for science and technology.

In some cases where fast non-destructive analysis is required, single-shot measurements become especially important. A review [46] is concerned with the complications caused by the lack of statistical averaging of the analytical signal, most all, the influence of signal fluctuations from pulse to pulse and the surface contamination on the quantitative determination of the composition. A paper on the application of LIBS in analytical chemistry was also published in the prestigious US journal '*Analytical Chemistry*' by Spanish scientists.[47]

A series of reviews deal with the use of LIBS for analysis of geological samples and other natural materials. Harmon *et al.*,[48] who described the application of LIBS in geochemistry, noted that this method is of interest as regards the design of portable real-time sensors operating in the field. In another paper, Harmon *et al.*[49] emphasized the specific features of qualitative analysis by LIBS in geo-

chemical studies for obtaining the fingerprints of geological objects. In view of the variety of LIBS applications for geochemistry, the new term GEOLIBS was introduced in a review[50] of US scientists. This review considers the potential of LIBS for investigation of natural waters, minerals, rocks, soils, sediments and other environmental samples. Senesi[51] published an extensive review dealing with investigation of terrestrial and extraterrestrial objects with the attention being focused on a qualitative and quantitative analysis of minerals and rocks. Recently, Chinese authors[52] described the application of LIBS for analysis of geological samples.

The purpose of the present review is to demonstrate the successful use of LIBS in qualitative and quantitative analysis of environmental samples involving application of advanced data processing techniques for sample classification, identification of elements and spectral lines and improvement of the figures of merit of analytical data. The achieved limits of detection of most elements in soils, natural waters and other environmental samples are critically considered.

II. Fundamentals of laser-induced breakdown spectrometry and the instrumentation used

II.1. Physical principles

The interaction of a laser beam with matter starts with absorption of the radiation by the sample surface. According to calculations, this produces a $\sim 10^4$ K temperature of surface electrons in only $\sim 10^{-13}$ s. It is considered that phonons of the crystal lattice do not absorb the energy of laser radiation quanta.[53] The absorbed radiation is thermalized over time periods of $\sim 10^{-12}$–10^{-11} s and, as a consequence, the sample surface layer is strongly heated. As some critical value of the power density is achieved, laser-induced plasma is generated, which is accompanied by ejection of the matter from the surface. All involved physicochemical processes are usually referred to as laser ablation.

So-called thermal model satisfactorily describes laser ablation induced by most common nanosecond lasers.[54] The fast local heating of the substance triggers a cascade of laser-induced processes:[54–56]

— absorption of laser radiation by electrons;
— emission of neutral and charged particles;
— heating, melting and evaporation of the solid;
— shock and acoustic wave generation;
— deformations and thermally induced fracture of the solid;
— ejection of the matter from the surface;
— formation and expansion of the near-surface plasma;
— surface shielding by the plasma;
— laser radiation absorption by the plasma and heating of the plasma up to temperatures of $\sim 10^4$–10^6 K;
— chemical reactions in the boundary layer of the plume.

As the power density on the sample surface becomes $> 10^6$ W cm^{-2}, the melt starts to be displaced from the crater under the action of vapour pressure. This is accompanied by ejection of drops to the plasma and formation of a rim around the crater.[55,57] In the case of a further increase in the power density up to 10^8–10^9 W cm^{-2}, the temperature of the molten substance may reach a critical value, resulting in the explosive volume boiling accompanied by ejection of particles of various sizes.[56–58]

In the case of picosecond or shorter laser pulses or at the beginning of interaction with a nanosecond laser beam, the ablation kinetics has specific features that cannot be described in terms of the conventional thermal model. It was shown[59] that the lattice temperature in the beginning of absorption differs substantially from the temperature of electrons. In view of this fact, for subpicosecond laser interaction, a two-temperature ablation model was proposed,[54] which found a lot of experimental evidence. In the first tens of femtoseconds, a hot electron gas and a cold lattice coexist in the $\sim 10^{-9}$–10^{-7} m-thick surface layer of the sample,[60] which induces explosive ejection of hot electrons with simultaneous destruction and expulsion of the cold material of the crystal lattice. In this case, plasma is formed directly from the solid without melting. The absence of the melting stage is supported by the absence of the crater rim.[61–63]

It is evident that in terms of both thermal and two-temperature models, during the lifetime of the laser plume, many processes occur out of equilibrium.[64] This, apparently, accounts for the fact that the existing laser ablation models are unable to predict important analytical characteristics such as the mass of the sampled material, types of ejected species or its content in the laser plume for a particular pulse. These characteristics are affected by the laser radiation parameters and focusing,[65] the composition and pressure of the surrounding atmosphere[66] and, of course, by thermal and optical properties of the substance.[54]

From the analytical standpoint, the most important stage of laser ablation is the formation and evolution of the plasma plume, because it is the source of the emission signal. The key parameters of a laser plasma are the temperature and electron density. The methods of plasma diagnostics for determination of these parameters are described in detail.[67]

When nanosecond pulses are used, the vapour in the vicinity of the sample surface is heated to a high temperature and ionized in 3–5 ns. This results in breakdown and ignition of a plasma, which absorbs some of laser radiation due to the inverse Bremsstrahlung and photoionization. Since laser radiation reaches the surface only partially, the so-called plasma shielding preserves up to 80% of the pulse energy in plasma, which results in a considerable increase in its temperature (up to 10^5 K) and electron density (up to 4×10^{21} cm^{-3}).[65] Therefore, during the first 50–200 ns, the spectrum exhibits a continuous intense background caused, first of all, by the Bremsstrahlung and recombination processes and extremely Stark-broadened emission lines (up to tens nanometres).

During a femtosecond pulse, there is no enough time for matter to move from the sample surface to the environment; therefore, the laser pulse does not interact with the plasma. A fast electron cloud (10^7 m s^{-1}) several micrometres high appears above the surface under picosecond pulses; this cloud can interact with laser radiation. The geometric dimensions of the plasma are smaller when the sample is ablated by pico- and femtosecond lasers due to the lower pulse energy and the absence of plasma heating stage; hence, the continuous background intensity is lower and the plasma lifetime is shorter.[30] The initial conditions in the plasma depend considerably on pulse durations; however, in

the late time periods ($\sim$10 ns after the pulse), the radiation intensity is mainly determined by the energy accumulated in the plasma.[68]

II.2. Optical schemes used in laser-induced breakdown spectrometry

Before describing the instrumental approaches that can improve the figures of merit of the method, we consider the typical block diagrams of the LIBS instruments, which comprise the following principal parts:

— pulsed emission laser(s) for plasma generation;

— system for beam focusing on the surface (or in the bulk);

— emission collection system;

— spectral instrument with emission detector;

— devices for synchronization of the laser and detector, spectra recording and storage.

In the simplest and most popular optical configuration of LIBS, the laser is directed perpendicularly to the sample surface by mirrors and focusing optics (Fig. 5 *a*). The optimal focus position is 2 – 6 mm below the surface. The laser-induced plasma emission is collected by a one- or two-lens condensers directly to the entrance slit of the spectrometer or to the input face of an optical fibre. This design is suitable for ablation by double pulses generated in the same optical cavity of the laser where the delay between the pulses is several tens of microseconds (double-pulse LIBS). Two different beams (Fig. 5 *b*) are combined, most often, using a polarizing cube for the same wavelengths or semitransparent mirrors (for different ones). This enables variation of the pulse delay in the range from several nanoseconds to tens of microseconds. In the orthogonal configuration of the double-pulse LIBS (Fig. 5 *c*), one beam is directed perpendicularly to the surface, while the other beam (or a part of radiation deflected from the first laser by beamsplitter) is directed parallel to the surface through the laser plasma generated by the first pulse. To decrease the crater size, it is expedient to use UV radiation, for example, the fourth harmonics of a Nd:YAG laser, for the perpendicular maximal energy of the second pulse is preferable in this case to induce breakdown in the gas environment.

The remote LIBS measurements with direct plasma emission observation through a gas or air medium are performed using a Newton or Cassegrain telescope (Fig. 5 *d*) with a parabolic or spherical mirror; the laser radiation is directed to the sample by a system of lenses, *e.g.*, Galilean telescope. In the ChemCam instrument,[69] the plasma emission is focused and collected by means of a single system of mirrors and optical elements.

Another option for remote LIBS measurements is the use of an external probe connected *via* an optical fibre to the basic components of the instrument (Fig. 5 *e*). The external part comprises lenses that are selected depending on the numerical aperture of the optical fibre and the working distance from its end to the target. In this case, the laser and plasma radiations move along the same optical path in the opposite directions. The light beams are separated using an pierced aluminium mirror or a broad-band beamsplitter. Cuñat *et al.*[70] proposed a simplified optical system for the external probe: after the optical fibre, the beam was focused on the sample surface, while the plasma emission was collected directly on the input face of another fibre. The

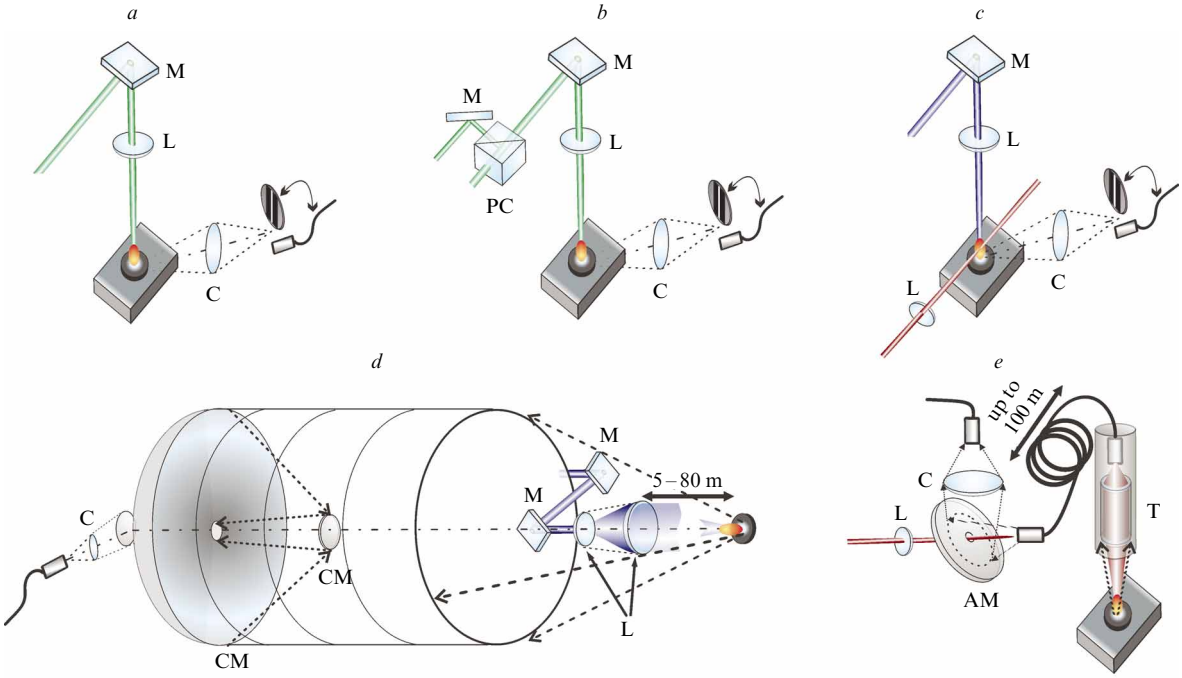


Figure 5. Typical optical configurations of LIBS systems using one (*a*) or two lasers in collinear (*b*) and orthogonal (*c*) configuration, the open-path configuration for remote LIBS measurements with direct observation of plasma radiation (*d*) and a configuration for remote LIBS with an external probe connected *via* an optical fibre cable to the basic components of the instrument (*e*).
The following designations are used, M are dichroic mirrors for laser radiation, L are lenses for laser beam focusing, C are condenser lenses for collection of plasma radiation, PC is a polarizing cube, CM are concave mirrors, AM is pierced mirror, T is two-lens telescope.

sensitivity of this system was sufficient for inspection of speleothems in the interior of caves based on the ratio of major and minor components.

II.3. Progress in instrumentation for laser-induced breakdown spectroscopy

The development of LIBS largely relies on the advancement of the equipment, first of all, lasers, spectral instruments and detectors. Rakovský *et al.*[71] comprehensively considered new laser sources: diode-pumped solid-state lasers, microchip and fibre lasers. They provide higher-quality beams, while reducing energy expenditure and cooling requirements. It is expected that the use of these lasers would ensure a similar performance of portable and laboratory devices.

The workhorses of the LIBS analysis of enviromental samples are Czerny – Turner or Echelle spectral instruments. Detailed description of their advantages and progress in miniaturization of the instruments are presented in mongraphs.[1, 33] Nevertheless, development of compact high resolution and high aperture spectrometers for portable field systems is still a topical task. Gupta and Peng[72] predicted the possibility of attaining 100% diffraction efficiency of transmission gratings. Numerous research resulted in the fabrication of a grating with an efficiency of up to 93.7% in the UV range,[73] which made it possible to manufacture compact high-aperture spectral systems. In remote LIBS measurements[74] with a spectrometer equipped with a transmission grating, the signal to noise ratio increased 3.6-fold. However, currently, there are no commercial gratings with large numbers of grooves efficiently operating at < 250 nm, which holds up the use of such gratings in LIBS.

A substantial miniaturization can be achieved by using heterodyne spectral instruments combining dispersive and interferometric elements. Combination of the Fabry – Perot etalon with a Czerny – Turner spectrograph produces a two-dimensional image in the focal plane, which represents parts of interference rings cut by the entrance slit;[75] thus, a spectrum corresponding to the resolving power of the spectrograph is observed in the horizontal direction, while the fine structure of this spectrum in a narrow spectral range is depicted vertically. As a result, a mercury doublet at 313.184 and 313.156 nm was resolved in a LIBS analysis of natural cinnabar.

Riebe *et al.*[76] proposed an interesting design with the successive arrangement of a first-order diffraction grating, a Fabry – Perot etalon and a prism. The simultaneous use of a grating and a prism provides the possibility to balance the resolving power over the whole spectral range. For example for a 50 μm and 7 mm high slit, a resolution of 0.051 – 0.063 nm was achieved in a wavelength range of 500 – 650 nm, which is close to the parameters of most popular Echelle spectrographs. Owing to the large slit size, a good sensitivity of the LIBS-system could be expected; however, the determination of the trace components can be hampered by the artifacts with a periodic structure in the spectra. An attempt was made[77] to use in LIBS the Michelson interferometer in which the mirrors are replaced by diffraction gratings mounted at angles slightly deviating from 90°. The resulting interference pattern was fairly intricate due to superimposition of bands inclined at different angles depending on the wavelength. This necessitated the use of Fourier transformation for interpretation. A resolution of 0.4 nm was achieved (in the 500 nm region) at a spectral window of 250 nm, which corresponds to characteristics of portable spectrometers manufactured by Ocean Optics and StellarNet companies (USA). The drawbacks of this system are complicated wavelength calibration and interpretation of interference patterns of multicomponent samples with rich spectra, for example, soils.

The sensitivity of LIBS systems is determined, to a large extent, by the detector. Multichannel detectors usually equipped with an image intensifier are most widely used. It is noteworthy that intensified cameras are expensive and should not be exposed to ionizing radiation, for example, in a radiative zone or in open space. There is demand for an inexpensive sensitive detector capable of signal gating in a microsecond range. The simplest solution is using a synchronized CCD camera;† in this case, due to electronic features, an intrinsic response delay of not less than 1 – 3 μs appears. However, with all other experimental conditions being equal, the limits of detection are at least an order of magnitude lower when an intensified CCD (ICCD) is used.[78] Apart from signal intensification, the sensitivity can be increased by elimination of noise sources. For example, signal accumulation from several pulses directly on the detector reduced the readout noise, which enabled determination of silver traces in soils.[79] For improving the signal to noise ratio in the LIBS analysis of samples submerged in water, Sakka *et al.*[80] proposed the acousto-optic modulator for time-gated measurements instead of image intensifier. A drawback is the low effective transmission coefficient, which also depends on the wavelength.

An alternative to intensifiers is provided by the electron-multiplying CCD (EMCCD), which can substantially amplify the signals. In order to suppress false signals due to the dark current amplification or readout noises, a strong cooling of the array (down to -70 °C) and an increase in the effective exposure time (up to milliseconds) are required.[81] Furthermore, signal amplification in each register is random and can distort the ratio between the spectral lines. Nevertheless, by using EMCCD, it was possible[3] to classify rocks without interference from the intense lines of the matrix. In recent years, CMOS arrays have been developed,‡ which are not inferior to CCD as regards the quantum efficiency and the area of photoactive region. The use of CMOS arrays seems most promising owing to their advantages such as random access to pixels for acquisition of only required data, the possibility of combining the image sensor and signal processing functions within the same circuit, which results in miniaturization and lower cost of the cameras. The single-photon avalanche diodes (SPAD) array fabricated in a CMOS technology resulted in a detector with a performance similar to ICCD systems (a gate down to 0.7 ns with temporal resolution down to 250 ps); the use of this detector in LIBS was demonstrated[82] in relation to analysis of the mineral barite.

Finally, we would like to note that the LIBS instrumentation and optical designs are also suitable for Raman spectroscopy. Quite a number of Raman – LIBS hybrid systems have now been developed for geological and outer space studies; they can simultaneously provide information on the elemental and molecular composition of rocks and minerals.[83]

† Charge-coupled device.

‡ Complementary metal – oxide – semiconductor structure.

III. Qualitative analysis

III.1. Elemental analysis

The spectra of laser plasma bear information on the presence of particular component in the sample by specific set of emission lines of each element and the line intensity being proportional to the component content. As a rule, the purpose of qualitative analysis in LIBS is to determine elemental composition and, in some cases, the chemical species in which the element exists in the sample. Sample classification for a restricted range of objects, for example, the determination of the type of rock, the provenance of a mineral and so on can be distinguished as a separate task of qualitative analysis (sample classification using LIBS is shown below).

For performing qualitative elemental analysis, it is necessary to identify the atomic lines in the spectrum. This is usually done by using atomic spectral databases: NIST [84] and Kurucz [85] databases and, much more rarely, the van Hoof database.[86] The numbers of known atomic spectral lines in these bases are 140 000, 450 000 and 920 000, respectively. Since geological samples are complex heterogeneous objects containing ten to twelve major elements including elements with rich emission spectra (iron, titanium), correct line identification is quite a challenge. In the opinion of American spectroscopists Cremers and Radziemski,[34] pioneers of the LIBS technique, the line assignment is a blend of science, art and experience, because the following factors are to be considered together:

— knowledge of the sample in order to rule out obviously false identifications, for example, detection of promethium or technetium lines in the spectra of natural samples;

— relative line intensities from spectral databases;

— the presence of spectral lines of various ionized states depending on the experimental conditions; lines of neutral or singly ionized species are usually observed in air, while even quarterly and quintiply ionized species can be detected in vacuum;[87, 88]

— observation of combinations of intense lines and especially multiplets: if one of the transitions appears, the other transitions must also be present in the spectrum.

In view of the foregoing, Fichet *et al.*[89] recommend unambiguous assignment of at least three lines for reliable identification of an element in a solid or liquid sample. However, in the case of remote analysis, the line intensity rapidly decreases. Therefore, in a study of Sallé *et al.*,[90] in which the plasma was located > 8 m away from the radiation collection system, only the most intense lines of the major components were observed, and they were used for element identification in the rocks.

To simplify the line assignment procedure for the spectra of laser-induced plasma, automated (semiautomated) identification algorithms have been suggested. Mateo *et al.*[91] developed the SALIPS software package, which generated spectra using the relative intensities of atomic lines taken from the NIST database,[84] while the line width selection and line intensity were fitted to experimental data manually. Thus, identification of the spectra consisted in visual comparison of the synthetic and experimental spectra in the specified spectral range. A procedure of this type requires preliminary assignment of the most intense atomic lines by the operating person and is actually only an accessory tool for assignment of weak spectral lines.

Ukwatta *et al.*[92] proposed an interesting approach to determination of the elemental composition of the sample without converting the CCD-detector signal to the spectrum. In this case, a special metrics was calculated to evaluate the similarity between the binary data describing the digital image of the spectrograph focal plane and the image of the theoretical spectrum simulated by means of the NIST database. Unfortunately, the proposed algorithm proved applicable only to identification of pure substances and failed to identify individual components even in binary mixtures.

Another algorithm for identification of spectra without considering the physical essence of the spectral information [93] is based on ranking the importance of information in the text retrieval. In this case, the element was taken as a document, the peaks were taken as words and the test sample was the query. The authors calculated a metric called weight, which was directly proportional to the peak intensity and inversely proportional to the number of peaks in the close vicinity to it. This does not seem sufficiently substantiated for line identification because in the case of elements with rich spectra, the 'weight' of particular lines decreases. Apparently, this accounts for the fact that matrix elements like manganese and nickel often cannot be identified. Restriction of the number of element candidates to twelve [94] and upgrade of the algorithm to include the distance between the observed peak and a nearby spectral line in the database allowed correct determination of all elements in the synthetic spectra. However, it seems rational to follow the approach proposed by Miles and Cortes,[95] who suggested the MP metrics to assign the lines in the spectra of soils:

$$\mathrm{MP} = \frac{c_n}{|\lambda_m - \lambda_{\mathrm{theor}}|} \qquad (1)$$

where c_n is the element abundance in the Earth crust; λ_m and λ_{theor} are the wavelength of the observed peak and the spectral line from the database, respectively.

The line was identified automatically if the MP value was at least three times greater than those of other possible candidates.

The laser plasma temperature varies over a broad range, from 3000 to 20 000 K, which additionally complicates the correct line assignment even for one-component samples. Modern databases can serve to generate the synthetic spectra of single elements for certain temperature and electron density,[84] which still does not rule out incorrect interpretation even in the case of one component. As an example, Fig. 6 shows the experimental and simulated spectra of pure iron for various temperatures. It can be seen that the real spectrum corresponds more closely to the line ratio calculated for 6000 K, although the laser plasma temperature can be much higher (upon evaporation of rock samples, it reaches 17 000 K).[96] Furthermore, the simulated spectra do not show the transitions for which the Einstein coefficients are unavailable, *e.g.*, the fairly intense Fe I line at 542.41 nm. Fantoni *et al.*[97] used a similar approach for interpretation of the spectra of multicomponent natural samples. First, few lines of the major components sufficient for calculating the plasma temperature were identified semiautomatically using the dedicated application developed in the LabVIEW enviroment. Then the given temperature and expected instrumental line width were used to generate

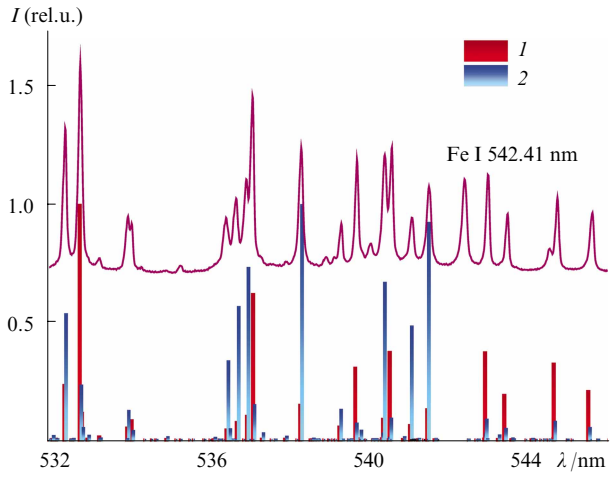


Figure 6. Experimental (above) and simulated (below) iron spectra for temperatures of 6000 (*1*) and 12 000 K (*2*).

multiple-element spectra that were afterwards compared with experimental data. This made it possible to determine the elemental composition of sea sediments (Ca, C, Mg, Mn, Si, Al, Fe, Ba, Ti, Na, K) and to semi-quantitatively estimate the excess over the threshold values of the regulatory requirements in the Antarctic by underwater LIBS.[39]

Apart from a highly variable temperature, laser plasma has a relatively high electron density ($10^{16}-10^{19}$ cm^{-3}). Hence, the Stark effect has the most pronounced influence on the shapes and positions of emission lines, which may often result in incorrect line assignment. It was noted[98] that currently there is no commercially available software for automated line assignment considering the Stark effect. The authors recommend choosing late plasma observation times (this, however, reduces the sensitivity) and developing algorithms for interpretation of spectra taking account of the Stark effect.

Our task was to develop an algorithm for automated interpretation of spectra considering plasma characteristics and properties of spectral and recording equipment.[99] The algorithm is based on constructing a set of model spectra for various temperature and electron density combinations with the assumptions of local thermodynamic equilibrium, plasma homogeneity and the absence of self-absorption and with allowance for emission line broadening and instrumental function. Then the Pearson correlation coefficients (R) for the experimental spectrum with each model spectrum were calculated. The lines were identified using the model spectrum best correlated with the experimental one. The line assignment in the model spectrum took account of the intensity ratios of transitions that fell into the region of the considered peak. Apart from automated identification of spectra without preliminary temperature and electron density calculations, this algorithm can be used to estimate these parameters of the laser plasma. Figure 7 shows the experimental spectrum of a soil and the model spectrum best correlated at a temperature of 0.65 eV and the electron density $\log N_e = 17.1$. In all, 69 peaks were detected and out of these, 64 peaks were successfully identified automatically by the above algorithm (see Table 1).[100]

An alternative approach that takes into account characteritics of the emission source is to compose a database of laser-induced plasma spectra. This protocol for automated processing of spectra is implemented in the software of the Applied Spectra company (US), a manufacturer of instruments for LIBS.[101] Under the supervision of Melikechi,[102] LIBS spectra of 40 elements were included into a database. It was shown for sulfur, selenium and iodine that the wavelengths and the relative intensities of transitions

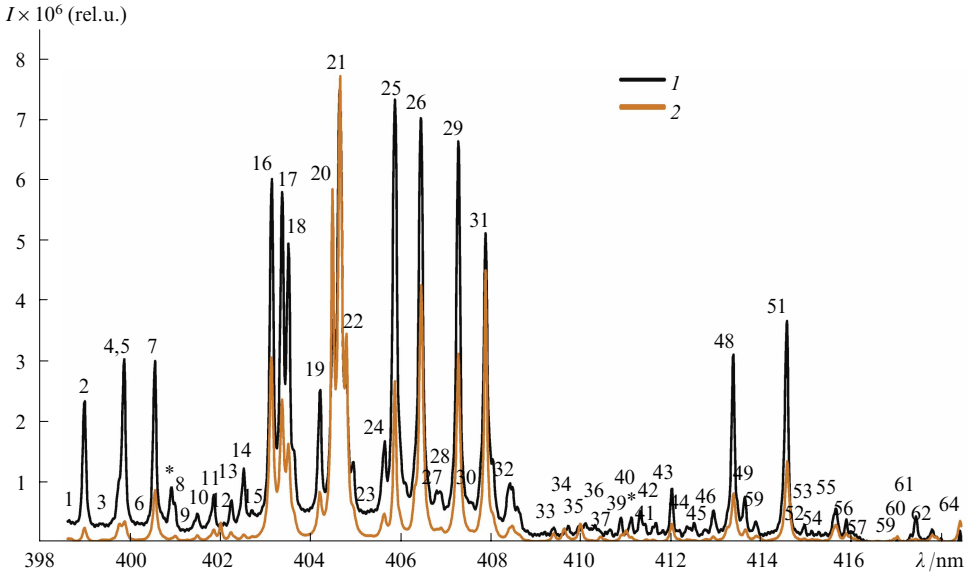


Figure 7. Experimental (*1*) and model (*2*) spectra of a soil sample.
Nd:YAG laser, 355 nm, power density of 5 GW cm^{-2}, delay of spectrum registration 3.5 μs, gate 2 μs; the line assignment is given in Table 1.

Table 1. Results of automated line assignment in the spectrum of a soil sample.[100]

Peak number	Species	Wavelength /nm	Peak number	Species	Wavelength /nm	Peak number	Species	Wavelength /nm
1	Fe I	398.617	23	Mn I	405.247	45	Fe I	412.562
2	Ti I	398.976		Fe I	405.272		Fe I	412.618
3	Fe I	399.401	24	Mn I	405.554	46	Fe I	412.761
	Fe I	399.401	25	Pb I	405.781	47	–	
	Fe I	399.411	26	Fe I	406.359	48	Fe I	413.206
	Ca I	399.461	27	Fe I	406.698	49	Fe I	413.468
	Ti I	399.469		Fe I	406.727	50	Fe I	413.700
4	Fe I	399.739	28	Fe I	406.798		Ca I	413.789
5	–	–	29	Fe I	407.174	51	Fe I	414.387
6	Fe I	400.166	30	Fe I	407.479	52	Fe I	414.767
7	Fe I	400.524	31	Sr II	407.771	53	Fe I	414.937
8	Fe I	400.971	32	Mn I	408.294	54	Ca I	415.025
9	Ti II	401.239		Mn I	408.363		Fe I	415.025
10	Fe I	401.453	33	Ca I	409.263	55	Ti I	415.096
11	Mn I	401.810	34	Ca I	409.493		Fe I	415.390
12	Pb I	401.963	35	Ca I	409.853		Fe I	415.450
13	Fe I	402.187	36	Si I	410.294	56	Fe I	415.680
14	Fe I	402.473	37	Fe I	410.411	57	Fe I	415.778
15	Mn I	402.643	38	–	–	58	–	–
16	Mn I	403.075	39	Ca I	410.853	59	Mg I	416,727
17	Mn I	403,306	40	Fe I	410.980		Pb I	416.803
18	Mn I	403.448	41	Fe I	411.297	60	Fe I	417.090
19	Mn I	404.136	42	Fe I	411.445	61	Fe I	417,212
20	K I	404.414	43	Fe I	411.854	62	Fe I	417.564
21	Fe I	404.581	44	Fe I	412.180	63	–	–
22	K I	404.721		Fe I	412.251	64	Fe I	418.175

present in the NIST database [84] differ significantly from the parameters of experimental lines in the spectra of laser plasma.

The use of LIBS spectra of elementary substances has a drawback of substantial matrix effects, which affect the processes in laser-induced plasma. For example, the intensity of the ionic lines S II 545.38 and 564.0 nm is two to three times higher in the spectra of sulfide minerals than in the spectra of sulfate-containing samples for nearly the same sulfur content.[103] The use of aqueous solutions of salts minimized the discrepancies between the experimental line positions (to not more than 15 pm) in the spectra of laser-induced plasma and NIST data for 46 elements.[89] In a publication [104] devoted to determination of samarium, europium and gadolinium in waste water, the lanthanide lines were also assigned using the spectra of solutions of individual substances. As a result, in addition to correct spectral line identification, the spectral ranges for quantitative analysis with minimum spectral interferences were chosen.

III.2. Discriminant analysis

It has been noted above that LIBS is now actively used for classification of environmental samples. In this problem, the initial data is the matrix of the sample spectra $\widetilde{\mathbf{X}}$ (m rows correspond to particular m objects, while n columns correspond to the wavelengths). A special algorithm called a classifier [105] transforms every row vector of object features (spectrum) into an integer (number of the class) according to the numerical values of the features (in the case of LIBS, intensities for different wavelengths). The number of variables n in the LIBS data can be great (1000 and more); with increase in this number, the complexity of the classification problem grows exponentially (curse of dimensionality); therefore, various methods of data compression are used, most often, principal component analysis (PCA).

According to this method, a centred data matrix $\mathbf{X}$ is first calculated. Then new coordinates (basis) are determined as a set of a ($a < m$, $a < n$) orthonormalized and mutually orthogonal loading vectors or principal components (rows of the matrix $\mathbf{P}_a^T$) the direction of which is chosen in such a way as to maximize the sum of projections of the initial data (spectra) onto the first component, to minimize the sum of projections of residues (matrix $\mathbf{X}$ minus the product of the column vector of the first projections onto the first load) onto the second component, *etc.* (NIPALS algorithm [106]). These projections are called scores and they form the matrix $\mathbf{T}_a$. From the mathematical standpoint, the loading vectors are the eigenvectors of the covariance matrix for the transposed centred initial data matrix $\mathbf{X}^T$. The number a is called the effective (chemical) rank of the matrix $\mathbf{X}$. Each principal component describes the variation of the initial data for different wavelengths n. Thus, the matrix $\mathbf{X}$ is represented in the form

$$\mathbf{X} = \mathbf{T}_a\mathbf{P}_a^T + \mathbf{E} \qquad (2)$$

The matrix of formal variables $\mathbf{T}_a$ is actually a new matrix of signals in the principal component space bearing all useful information contained in the initial data. Meanwhile, it has a much lower size than n: the number of non-zero

variables of each object (row vector) is equal to the number a of calculated loads. Correct choice of the number of principal components is very important as this determines what should be taken as useful data and what is noise (residual matrix **E**). The a value is selected for each particular problem, for example, based on dispersion analysis of the residues, analysis of the lengths of score vectors (columns of matrix $\mathbf{T}_a$) called also singular values. The PCA method is often utilized in LIBS in order to visually demonstrate the possibility of object classification.[107–113] In this case, the score plot is constructed (most often, in the space of the first and second principal components) and attempts are made to distinguish groups of points (areas) in the plot.

Another method for decomposition of multivariate initial data is the projection on latent structures (PLS),[106] which is used in two alternatives (PLS1 and PLS2). In this case, regression is performed for both the matrix of predictors (signals) and the matrix of responses (component concentrations in the samples), and the projections (scores for both matrices) are constructed consistently. In LIBS, partial least squares discriminant analysis (PLS–DA) is used most widely.[3, 107, 112–115] This algorithm makes use of PLS2 decomposition followed by construction of regression between the matrices of signals and dummy responses.§ Other classification methods are rarely used: linear discriminant analysis (LDA),[108] LDA preceded by PCA data compression (PCA–LDA),[116] soft independent modelling of class analogies (SIMCA),[109] the k-nearest neighbours (kNN) method[49] and the support vector machine (SVM) method.[117] All these methods refer to the group of training-based classifications, *i.e.*, they imply the presence of a training ($\mathbf{X}_c$) and test (or validation) ($\mathbf{X}_t$) data sets for which the class of objects is known beforehand. The classification model is constructed using the set $\mathbf{X}_c$, its quality (the percentage of correctly classified objects) being evaluated by application to the set $\mathbf{X}_t$. After that, it is decided whether or not the classifier can be applied to unknown objects.¶

Below the use of the above classification methods in LIBS is considered in more detail according to the types of problems being solved. One of the problems is identification of conflict minerals — classification according to their geographic origin. Alvey *et al.*[113] used PLS–DA to classify 157 garnet samples from 92 locations all over the world. The set comprised six garnet mineral types differing by the contents of major (Ca, Cr, Mn, Fe, Si, *etc.*) and minor (Na, K, Li, H) elements. The spectra were recorded using a commercial LIBS-2500+ system (Ocean Optics, USA), which covers the 200–960 nm range (~0.1 nm resolution) and has 13699 channels for recording intensity at different wavelengths in a single measurement. Classification in terms of the garnet type was performed. As noted by the authors, this rather trivial problem can often be solved by visually comparing the spectra (especially if the distinctive component is present in the sample), because intense lines of the major components are used. However, the idea was to automate the process in order to reduce the time of routine analysis for a large number of samples. The matrix of predictors was composed of 25 spectra for each sample containing only lines of the elements at the chosen wavelengths (altogether ~150 lines). The set included the nitrogen atomic lines, which is not quite reasonable, because the assay was performed in air. The number of latent variables in the PLS2 regression was chosen by leave-one-out cross-validation.[117] The classification results for the 25 single spectra for each sample were subjected to a simple voting procedure to determine the sample type: the sample was assigned to the class to which most of its 25 spectra were attributed upon classification. According to the highest percentage of correctly recognized samples (~95%), the optimal number of latent variables was found to be 26. This quantity was, apparently, overestimated (the model was overfitted), as the differences between classes of samples were determined by seven or eight elements and the number of considered classes was not higher than six. It is not entirely clear why the authors used the leave-one-out cross-validation instead of splitting the whole set and the corresponding spectral data into blocks, although they had approximately 25 samples of each type. The authors did not use any algorithms for choosing the number of components. Moreover, Wold *et al.*[117] did not recommend the cross-validation to be performed with removal of only one sample.

Since the cross-validation errors are random variables and are subject to inaccuracy, it is possible to estimate the significance of adding a new component to the model by statistical comparison of the errors with one another or with their standard deviations.[118, 119] For example, in a quantitative LIBS analysis of steels,[120] the overfitting was avoided by using an F-criterion-based algorithm, which estimated the difference between the results of prediction responses during cross-validation for different numbers of components.[119] For more reliable evaluation of classifier quality, the initial set can be split into training and validation sets.

Classification of garnet samples in terms of the provenance, *i.e.*, the geographical location of the mineral deposit, is a much more complicated task than the classification in terms of the mineral type, since in this case, the spectral differences are caused by minor and trace components.[113] First, the samples were divided according to the mineral type and then the geographical location discrimination (from 2 to 5 depending on mineral type) was performed within each group. Samples were included into the set if their number was at least three for one geographical location (altogether 87 samples).The average percentage of samples with correctly recognized geographical locations was 45%; for some garnet types, discrimination errors reached 100%, which is attributable to a small number of samples of particular classes in the training set. Analysis of the contribution of each variable of the predictor set to the model scores demonstrated that minor components (Na, K, Li, H) are responsible for the geographical location. The results concerning mineral classification in terms of the provenance may possibly be improved by using the full spectra as the initial data (after getting rid of noise) and by utilizing the approach reported by Pomerantsev,[105] which

§ Matrix in which the columns correspond to the number of the class of object, and the element is unity if the object in the row belongs to this class and otherwise it is zero.

¶ Chemometric methods are described in detail in the monograph by Pomerantsev [105] and on the website of the Russian Chemometric Society (http://rcs.chemometrics.ru/english.htm). Useful information and references and implementation of some algorithms can be found on the website http://classifion.sicyon.com/About/index.htm. The separate website — http://www.support-vector-machines.org/index.html — is devoted to the SVM method.

implies the PCA decomposition of the matrix of dummy responses with subsequent LDA analysis.

A study [114] is devoted to geographical discrimination of 14 columbite and tantalite samples (niobium and tantalum ores, respectively). LIBS analysis was performed using a commercial RT100-HP system (Applied Spectra, US) equipped with an ICCD. The system could provide both high- and low-resolution spectra. The authors used three initial data sets containing lines of major elements (Ta, Nb, Fe, Mn) and significant trace components (W, Ti, Zr, Sn, Ca, Zn, *etc.*), in particular, high-resolution (0.05 – 0.1 nm) data for two narrow ranges (235 – 285 and 313 – 358 nm) and low-resolution (0.2 – 0.3 nm) data for a wide range (250 – 490 nm). Forty spectra were recorded for each sample, each spectrum being normalized to the integral intensity (the sum of the recorded intensities for all wavelengths). The number of PLS – DA latent variables was selected and the classifier quality was verified in the same way as for the analysis of garnets. Using the voting procedure, correct assignment was obtained for 13 out of 14 samples for the narrow spectral ranges and for all 14 samples or the low-resolution wide ranges.

The works along this line were continued, and in 2012, classification results for 57 columbite – tantalite samples from 37 locations were reported.[115] The set of data for each sample comprised 100 spectra, each consisting of 1024 data points in a broad spectral range. Since for some deposits only one or two samples were present, the authors abandoned the leave-one-out cross-validation procedure for verifying the classifier but divided the data into 15 groups of approximately equal size and performed cross-validation with the removal of one group from the training set. Since the classification was performed for a single spectrum, the authors presented the cross-validation results including assignment of the spectrum to the sample, deposit and the country of provenance. The 50 principal components were chosen according to maximal percentage of correctly classified samples for particular discrimination task. This number of principal components may indicate the model overfitting. All of the samples were correctly assigned to geographical locations of the deposits. Nevertheless, it would be worth paying attention to the complexity of initial data (predictors) and selection of the number of components bearing useful information; the cross-validation used by the authors means the presence of the spectra of the sample both in training and validation sets, while the overfitted models may cause misclassification of fully independent validation set.

A multivariate classifier was used for provenance identification of sea salts from 11 locations (in France, Korea, Japan and China).[107] The number of components for the model was chosen relying on visual analysis of PCA loadings (rather than based on the maximum percentage of correct assignments upon cross-validation as in other publications [113, 114]). This approach is preferred, because it eliminates the principal components containing mainly noise. The cross-validation demonstrated that the PLS – DA model with five components ensured a 85% correct classification, despite the relatively narrow spectral range (771 – 798 nm). It was also shown that the salt manufacturing technique can be identified based on the aluminium line intensity in the spectrum.

One more class of problems being solved is the discrimination of minerals according to their mineral type. Usually, this implies the discrimination within a large class of minerals with a certain common characteristics (*e.g.*, with the same anion), or even larger groups are considered (*e.g.*, carbonates are combined with silicates) and classification is carried out in terms of all possible characteristics intrinsic in each single class. For instance, Harmon *et al.*[49] addressed both problems — classification within mineral groups with the same anion and classification in combined mineral groups (carbonates plus silicates, carbonates plus feldspars plus pyroxenes). The training set for each sample included 5 – 10 spectra in a wide spectral range — from 200 to 965 nm (0.1 nm resolution, 13 500 points). The distance between the test data and the training set spectra during cross-validation was estimated using Pearson's correlation coefficient (simple correlation method called also the nearest neighbour method). The assignment was considered correct if the best correlated test and training spectra had the same class. For the carbonate group, this verification showed a high level of successful classification ($\sim$96%), which can be attributed to pronounced differences between the spectra caused by cations (Zn, Pb, Mg, Ca, *etc.*). In the case of feldspars and pyroxenes, 86% and 84% of spectra, respectively, were correctly classified. In the combined carbonate + silicate group, cross-validation resulted in the correct identification of 98% of the spectra. Misclassifications may be attributable to mineral substitution in the samples or similar compositions of minerals. For instance, one spectrum of azurite $Cu_3(OH)_2(CO_3)_2$ was erroneously attributed to malachite $Cu_2(OH)_2CO_3$, while the spectrum of one silicate was confused with the spectrum of manganese carbonate due to the presence of manganese inclusions in the silicate. However, the application of the same correlation approach for classification of beryls (aquamarines, emeralds and so on generally described as $Be_3Al_2Si_6O_{18}$) was improper, only 50% of the spectra being assigned correctly. The differences between the classes are caused, in this case, by partial replacement of the Be^{2+} and Al^{3+} cations by Na^+, K^+, Rb^+, Mn^{2+}, Fe^{3+} and Cr^{3+} cations; furthermore, the chemical composition of even one type of beryls significantly varies. Therefore, other approaches to the classification are needed.

Two modifications for the correlation approach were proposed:

— k nearest neighbour classification method ($k = 5$);

— a chemometric approach [105] according to which all data are normalized, before correlation analysis, to the standard deviation at each wavelength.

The first approach even somewhat impaired the classification results, while the second one considerably improved the results, especially in the case of beryls and pyroxenes, by 10% and 12%, respectively. An extended PLS – DA study was carried out in LIBS systems (single- and double-pulse spectra, various detectors, system for remote analysis).[112, 121] In this case, groups of samples represented carbonates, fluorites, silicates and soils. The training set comprised 20 spectra and the validation set included 5 spectra for each sample. The maximum average dummy response value was used as a criterion for the assignment of a sample to a class. The number of components was chosen based on the best results achieved upon cross-validation; their number from 16 to 20 seems overestimated, since 92.4% of data variance is described by the first three components in the PCA decomposition. Moreover, clear sample differentiation is observed in the space of the first to

third principal components (PC1 – PC3). Moreover, 4 – 6 components describe 98% – 99% of the variance, and a further increase in the number of components actually adds mainly noise. Nevertheless, upon cross-validation, correct assignment reached almost 100%. The worst results were achieved in soil discrimination — an Echelle spectrometer system provided 75% of successful classification *versus* 50% for a system with several Czerny – Turner spectrometers. Averaging of the spectra improved the results by 10% – 15%.

A group of Chinese authors[3] analyzed the Triassic sedimentary rocks from the Sichuan Basin — 16 samples of limestones, spars, mudstone and marl. Ten stratigraphic locations of sampling served as classes. The samples were powdered or pressed into pellets; materials without sample preparation were also used. In order to reduce the effect of sample non-homogeneity, the spectra were acquired from 100 spots of the surface and were included into the set without preliminary processing. The predictive powers of the PLS – DA and SVM clsasifiers were compared for two different systems with the Echelle spectrometer and the Czerny – Turner spectrometer. The components were chosen and the PLS – DA model was evaluated by five-fold cross-validation in which the training set comprising 80 for each sample spectra was divided into 5 blocks; 20 spectra for each sample served as the test set. A sample was assigned to a particular class by the highest probability principle in the matrix of dummy responses. The chosen number of components for PLS – DA equal to 7 appears more adequate than the values in the above-cited publications.[112 – 115] Both classifiers demonstrated a 100% performance for most data sets except for two samples: a dark-purple marl and a grey limestone (10% – 60% of correct assignments), which is attributable to fairly similar geological conditions of rock formation. The elements Al, Si, Ca, Mg, Fe, K, Ti and O were found to be responsible for differences between the classes. A dedicated algorithm called variable importance in projection (VIP) scores[122] was used for reduction of the SVM classifier data set dimension to distinguish the variables responsible for the differences between classes ($\sim$3300 out of 29 800). Note that classification was correct for the samples with preliminarily polished surfaces, unlike pressed powdered samples. The authors explained this as being due to elimination of differences between the samples during grinding. The quantitative analysis is more correct for homogeneous samples with equal grain size for all samples; however, for discrimination it is more important to retain differences in the sample morphology — grain size, adhesion, *etc*.

A number of studies dealing with mineral and rock classification are related to the NASA mission on Mars, in particular, exploration of the planet surface by the Curiosity Mars rover since August, 2012.[26] One of the tasks set for the ChemCam instrument mounted on the rover is to determine the type of rock based on spectral data in order to evaluate the necessity of sampling and sample analysis by other instrumental methods inside the rover. Chemometric approaches are able to absorb new data obtained for the Martian surface into classification models upon mere addition of these data to the set of spectra obtained on Earth under conditions as close as possible to the Mars conditions.

A group of scientists[123] from the MSL (Mars Science Laboratory) team demonstrated a classification method in which discrimination was performed in the space of independent components [independent component analysis (ICA)].[124] The minimal Mahalanobis ($d^{1-\gamma}_{\text{Mahal}}$) or Manhattan ($d^{\gamma}_{\text{Manhat}}$) distance[105] between unknown and training spectra (namely, their projections) was used as the criterion for classification. The experiments mimicked the analysis conditions on Mars (9 mbar CO_2, 3 m distance to the sample) for a set of six samples forming a separate class (basalt, limestone, gabbro, *etc*.). Forni *et al*.[123] reduced sixfold the number of variables involved in the analysis as compared with the initial data set: only those channels were chosen in which the variance exceeded the total average variance (for the whole training set). The data were split 1000 times into sets composed of 30 training and 20 test samples and the classifier was constructed and tested. If the distance between the spectrum projections was beyond 99.999% of the confidential interval, the spectrum was regarded as unclassified and removed from the training set. The classifier performance can hardly be evaluated, because the results for the classified spectra are given without considering the imposed constraints and the percentage of unclassified spectra is indicated separately. Analysis demonstrated that even the fifth component actually describes the noise; however, the authors used eight components for analysis with contributions (γ) of both above-indicated distances (the product $d^{\gamma}_{\text{Manhat}}\, d^{1-\gamma}_{\text{Mahal}}$, $0 < \gamma < 1$). In the conclusion, it was indicated that the ICA classification is better (95% for $\gamma \approx 0.5$) than PLS – DA (86%). Unfortunately, little attention was paid to chemical and geological aspects of the problem and the choice of samples also remained obscure.

The classifiers based on artificial neural networks (ANN) rather than on data analysis in a new component space are also used for classification of mineral and rock types. The ANN fundamentals and applications in LIBS were reported by Koulejev and Lui.[125] The same researchers demonstrated[126] the performance of the ANN classifier in relation to geological samples. The training set consisting of 41 standard samples (rocks, sedimentary rocks, minerals, ores and soils) represented a separate class, *i.e*., the number of output neurons was 41. Independent data for training (20 spectra for each of five sample points) and testing (10 spectra for each of ten points) of a three-layer neural network were obtained. Out of a broad spectral range of 200 – 970 nm, the authors chose 139 lines weakly self-absorbed and well isolated spectral lines (139 input neurons). The results of testing of the trained network on 14 real samples were as follows: 88% of correct classifications upon averaging of the spectra from 10 laser pulses and 100% for averaging over 50 spectra.

One more type of classification problems that can be solved by LIBS is forensic examination, first of all, discrimination of soils in terms of location. It was shown[108] that the use of LDA provides an almost 100% correct assignment of soils taken from two different locations separated by $\sim$30 miles. In each location, 36 soil samples were taken according to a special pattern. Upon analysis of spectra, five intensity ratios of the lines of trace components and the sample matrix were chosen as LDA variables, namely, Sr II 421.6/Ti I 336.1, Ba II 493.4/Mg I 517.3, Ca I 643.9/Mg I 518.4, Fe I 495.8/Mg I 518.4 and Li I 610.4/Mg I 517.3. The authors demonstrated that LIBS can be used instead of LA – ICP – MS for forensic analysis of soils.

IV. Quantitative analysis

The efficiency of any spectral analysis is characterized by the accuracy of an analytical procedure. All types of quantitative measurements in LIBS are based on the relationship between the intensity of the characteristic emission of the element in the plasma and the element content in the sample (c). The intensity of the analytical line for quantification of the desired component can be expressed as:

$$I_i \sim f \eta c m_{\text{abl}} \exp\left(-\frac{E}{kT}\right) \quad (3)$$

where f is the emission collection efficiency, η is the atomization efficiency, m_{abl} is the ablated mass, T is the plasma temperature, E is the energy of the upper level.

Random variations of any of these parameters can substantially affect the repeatability of measurements. Pulse-to-pulse variations of the size, shape and the spatial position of the laser plume obviously affect the part of emission radiation that is imaged on the entrance slit. Furthermore, laser microanalysis is fairly sensitive to sample inhomogeneity. In turn, the intensity of the analytical signal of the element in plasma is related to the ablated sample mass, which depends on the laser radiation parameters (energy and focusing). Laser plasma characteristics, in particular, variations of the temperature, also influence the analytical signal.[127] The sample matrix has, most often, the most pronounced effect due to the differences in the ablation process.

Below we consider the experimental approaches that improve the precision of the analytical signal in LIBS and then the approaches to signal correction using an internal standard and statistical data processing for conventional calibration and quantification based on only spectral data and fundamental parameters (calibration-free LIBS) and multivariate calibrations.

IV.1. Improvement of the precision of laser-induced breakdown spectrometry

The repeatability of LIBS measurements is affected, first of all, by pulse-to-pulse fluctuations of the ablated mass and its fractional composition and by plasma formation and expansion into the environment.[127–138] Successive laser pulses on the surface form a crater rim due to displacement of the melt by the gas–vapour cloud.[128] In the case of ultrashort pulses resulting in minimal thermalization of laser energy at the surface or in the case of infusible materials, the rim is not formed.[129] The ablation of glassy materials affords cracks as a result of thermoelastic deformations,[130] while the ablation of organic materials, *e.g.*, leaves, produces traces of decomposition.[131] The explosive boiling of the melt accounts for the complex shape of the crater bottom with roughness of up to $\sim$0.5 μm in size.[57]

The use of femtosecond lasers for sample evaporation in an inert gas atmosphere under reduced pressure[61] may give craters of regular and, what is more important, reproducible shape. In the absence of the melting phase upon femtosecond laser ablation and, as a consequence, without ejection of the melt, the errors of analysis sharply decrease. Indeed, spatial distribution of sodium and potassium in mica plates[135] was investigated with resolution of 450 nm (the ablated mass was 220 ag) by the second harmonics of the femtosecond laser. One more unique feature of the femtosecond pulses is self-focusing of a beam giving rise to the filament — a plasma channel along the beam trajectory, which allows laser pulse propagation to the specified spot of analysis without significant energy loss or deviations caused by beam divergence and refraction.[136] The LIBS technique with such way of sample irradiation is called filament-induced breakdown spectroscopy.[137] It was demonstrated[138] that this approach can serve for environmental monitoring of urban air by quantification of toxic metals (Pb, Cu) in aerosol at a distance of up to 70 m with possible scaling up to a kilometre distance.

Alternatively to such expensive equipment, lasers operating in the ultraviolet range can serve to reduce the size and surface roughness of the crater.[132] For example, the fifth harmonics of an Nd:YAG laser was used for 3D imaging of a sample of the mineral bastnasite with 10 μm lateral resolution and 3 μm depth resolution.[133] Direct comparison of analytical characteristics obtained for IR (1064 nm) and UV (355 nm) laser radiation demonstrated that the best precision is achieved at 355 nm wavelength.[134] The advantage of UV radiation is related to decreased plasma shielding and increased contribution of photoionization processes in the transfer of the pulse energy to the sample. Hence, ablation by short-pulse UV lasers is a direct and the most efficient way to ensure high reproducibility of the crater size.

The ablation threshold can be achieved ahead of the lens focus, especially if aerosol particles are present above the sample surface. In order to exclude plasma movement and reduce the signal fluctuations, the focus is placed below the target surface; the optimal focus position depends on the experimental conditions and sample type and is usually 2 – 5 mm below the sample surface;[139] simultaneously, the analytical signal fluctuation (relative standard deviation) decreases from 15% – 42% to 1% – 4%.

Laser-induced plasma is spatially inhomogeneous and appreciably changes with time.[127] The variations of substance and temperature distributions in the plasma from one pulse to another can deteriorate the repeatability of measurements if only the central part of the plasma is considered; therefore, the condenser, which images the whole volume of the plasma to the entrance slit, is preferred.[140] However, in a study of element distribution profiles, this configuration would enhance the influence of edge regions, and, as a consequence, deteriorate the trueness and spatial resolution. A special chamber was proposed to decrease the contribution of emission from the laser plasma periphery and improve the capabilities of spatially resolved measurements.[141]

The environment affects the shape and parameters of the laser plume and, hence, the accuracy and precision of the measurements. Sallé *et al.*[142] demonstrated that the relative standard deviation (RSD) for the major and trace components change in different ways at atmospheric pressure in air and at a carbon dioxide pressure of 7 mm Hg: the precision of the trace component signal is higher in the former case, while the RSD is lower for the major elements in the latter case. This is attributable to lower self-absorption and less pronounced line broadening for major components and to the great expansion of plume particles at low pressure. Another obstacle is interaction of the plasma with the aerosol formed upon ablation, since the condensation of a vapour in the laser plume gives clusters.[54, 143, 144] It is noteworthy that material vaporization by UV radiation

decreases the average size and the overall number of clusters.[145] The average size of particles obtained by femtosecond ablation of bronzes is 2 – 3 times smaller than for nanosecond one, while the number of particles is 5 – 10 times higher.[146] Obviously, the errors introduced by the appearance of aerosol would be smaller for the use of femtosecond pulses.

Most of optical emission spectroscopy techniques use some kind of internal standard proposed back in 1929 by German physicist Gerlach.[147] The internal standard is also widely used in routine LIBS measurements. For instance, a procedure for arsenic determination in soils was markedly improved when the analytical signal was corrected to the iron line.[14] When laser ablation is used, experimentally measured characteristics (total plasma emission, acoustic wave, background emission and so on) often serve as internal standards in analytical atomic spectroscopy.[148] In order to avoid confusion, we will use the term 'internal standard' in its common meaning, namely, to designate the emission line of the sample component used for correction.

The descriptions of laser plasma often imply the presence of a local thermodynamic equilibrium. Despite the fact that matter and radiation cannot be described by the same temperature, the excitation kinetics is governed by particles of the matter and can be defined in terms of equality of the particle temperature and the 'excitation temperature'.[149] Subsequently, we use particularly this value as temperature (T). The intensity of an optical transition in a homogeneous optically thin plasma can be expressed as[150]

$$I = \frac{fhc}{4\pi\lambda}\frac{Agn}{Z}\exp\left(-\frac{E}{kT}\right) \quad (4)$$

where A is the Einstein coefficient for spontaneous emission, g is the statistical weight of the atomic state, n is the total number of element atomic species, λ is the wavelength, Z is the partition function. The intensity ratio of the lines of the analyte (A) and internal standard (B) has the form

$$\frac{I^A}{I^B} = \frac{n^A g^A A^A \lambda^B Z^B}{n^B g^B A^B \lambda^A Z^A}\exp\left(-\frac{\Delta E}{kT}\right) \quad (5)$$

As a rule, the internal standard is used to compensate the pulse-to-pulse variations of the analytical signal or matrix effects. These effects can also be suppressed by preparing synthetic reference samples which can be close to many types of materials. For example, geological samples were found to be adequately mimicked by silicate glasses doped with various amounts of analyte components;[2] materials of this type are used for *in situ* calibration in the LIBS measurements on the Curiosity rover.[151]

It can be seen from Eqn (4) that the temperature effect can be neglected if the upper electron levels of the transitions are close. Because of inhomogeneity of the plasma, additional limitations may arise in LIBS giving rise to spatial and temporal temperature and electron density gradients in the laser plume. In order to neutralize the temperature effect, Loge proposed successive correction algorithm making use of the 'instantaneous' temperature, which is employed to calculate the level populations.[152] In order to take account of the influence of plasma characteristics (temperature and electron density) on calibration employing internal standards, correction factors calculated by the Saha – Boltzmann equation were proposed.[153] The temperature and electron density for these calculations were determined independently. The use of normalized internal standard values made it possible to reduce the signal fluctuation from 14% to 5% and to considerably improve the calibration linearity (R^2 increased from 0.63 to 0.94).

The utility of the internal standard depends substantially on the emission line chosen. In the case of local temperature equilibrium, the general criterion of similarity of the upper levels (thermodynamic criterion) mentioned above actually specifies the necessary limitation for selection. Often, the thermodynamic criterion is sufficient (see, for example, Ref. 154). However, in some cases, the determination accuracy is deteriorated.[29] The use of the internal standard means that the reference line and analytical signal intensities are related to fluctuating parameters. Strict determination of this relationship based on the physical ablation model is impracticable; therefore, we proposed to find values and the analytical signal varying similarly with fluctuation of the laser plasma characteristics.[155] This problem was reduced to consideration of the correlation coefficient between the analytical line intensity and the emission signal intensity in each point of the spectrum. The reference line chosen in this way substantially improved the calibration for lead determination in soils. An alternative 'correlation' criterion for choosing the internal standard was postulated with the following key conditions:

— high correlation coefficient with the analytical line;

— the lines should be comparable in intensity

— whenever possible, the contents of the element used as the internal standard should not differ much in the analyzed samples.

The advantage of this criterion is that it can be applied both with and without local thermodynamic equilibrium. As an example, we consider the selection of the internal standard for molybdenum determination in soils and ores.[100] The correlation coefficients of the molybdenum analytical line for each point of the spectrum (correlation spectrum) are shown in Fig. 8 *a*. It can be seen that the iron line is most correlated, so it has been chosen as the internal standard for the calibration plot (Fig. 8 *b*). All points of calibration with this internal standard fall within the confidence interval. Zhang *et al.*[156] solved the inverse problem — the use of correlation analysis for selecting the analytical line to determine oxygen in coal with the reference line N I 746.8 nm. Oxygen atom lines with high correlation coefficients markedly improved the accuracy of analysis.

The signal fluctuations from one pulse to another have a significant effect on the precision of LIBS measurements under the optimal experimental conditions and with the use of the internal standard; therefore, various data processing procedures are utilized to improve the figures of merit. An algorithm proposed to subtract the background does not include consideration of its physical causes but allows automated processing of spectra with high and low noise levels. The use of this procedure substantially improved the accuracy of LIBS analysis of iron ore.[157] A similar algorithm was applied for signal correction in the analysis of a stalagmite surface.[158] It was shown [159] that while averaging the analysis data for natural minerals, one should take into account the grain size. Since the laser breakdown position in water is highly unstable and appreciably affects the repeatability, Lazic *et al.*[160, 161] developed a simple data processing procedure for underwater LIBS, which automatically eliminates the spectra that differ much in the plasma temper-

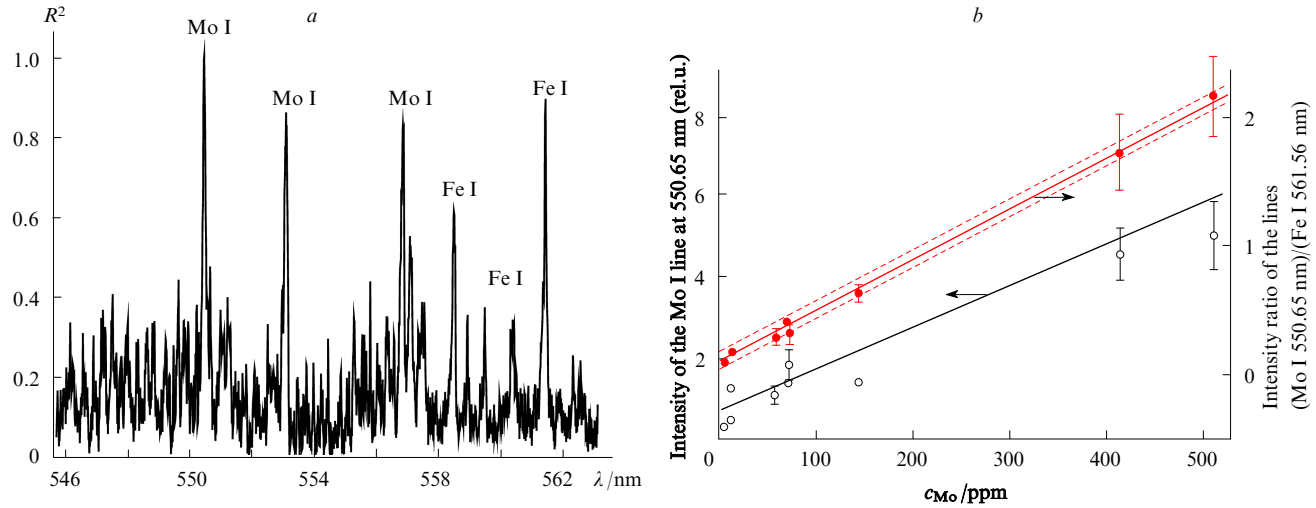


Figure 8. Correlation spectrum (*a*) and calibrations for determination of molybdenum (*b*).

ature determined from the continuum spectrum. The use of this procedure gave rise to linear calibrations that allow for direct quantitative analysis of samples submerged in water. In single-pulse LIBS measurements, the influence of surface contaminations or off-surface breakdowns is especially significant. Hahn *et al.*[162] developed a method for identification and removal of outliers, which substantially increased the signal to noise ratio. An algorithm of filtration of 'irregular' spectra,[163] in which outliers were identified by discrimination analysis techniques,[164] was proposed.

IV.2. Construction of multivariate calibrations

Decomposition of an initial data matrix followed by regression analysis is widely used in the quantitative LIBS analysis. The key methods are principal component regression (PCR) and partial least squares regression (PLSR). They provide for accurate results when analytical signals highly overlap. A model is constructed with the training set and evaluated by the test set; the selection of principal components is based on estimation of the residual variance upon initial data decomposition and calculation of the root-mean-square error of calibration (RMSEC) and the root-mean-square error of prediction (RMSEP) of training and testing.[105] After that, the regression model is applied to predict the component contents in the unknown sample. For example, in PCR, the component concentrations in an unknown mixture can be found by solving a system of matrix equations

$$\begin{cases} \mathbf{X}_c = \mathbf{T}_c\mathbf{P}^T = \mathbf{C}_c\mathbf{S} \\ \mathbf{X}_t = \mathbf{T}_t\mathbf{P}^T = \mathbf{C}_t\mathbf{S} \end{cases} \tag{6}$$

where $\mathbf{X}_c$ and $\mathbf{X}_t$ are centred matrices of the spectra of calibration and unknown (or test) samples, $\mathbf{T}_c$ and $\mathbf{T}_t$ are the score matrices for calibration and unknown (or test) data sets, $\mathbf{P}^T$ is the loading matrix [see formula (2)], $\mathbf{C}_c$ and $\mathbf{C}_t$ are centred matrices of concentrations of calibration and unknown (or test) mixtures, $\mathbf{S}$ is the matrix of pure component spectra. Note that signals and concentrations of unknown samples are centred against the same coordinate space as the calibration data, *i.e.*,

$$\mathbf{X}_t = \widetilde{\mathbf{X}}_t - \widetilde{\mathbf{E}}_t\,\mathbf{mean}(\widetilde{\mathbf{X}}_c) \tag{7}$$

$$\mathbf{C}_t = \widetilde{\mathbf{C}}_t - \widetilde{\mathbf{E}}_t\,\mathbf{mean}(\widetilde{\mathbf{C}}_c)$$

where $\widetilde{\mathbf{E}}_t$ is the unit column vector with a number of variables equal to the number of unknown mixtures, **mean** $(\widetilde{\mathbf{X}}_c)$ and **mean** $(\widetilde{\mathbf{C}}_c)$ are row vectors composed of column-average values of the matrices $\widetilde{\mathbf{X}}_c$ and $\widetilde{\mathbf{C}}_c$, respectively. From the first equation of system (6), $\mathbf{P}^T$ is expressed as

$$\mathbf{P}^T = \left(\mathbf{T}_c^T\mathbf{T}_c\right)^{-1}\mathbf{T}_c^T\mathbf{C}_c\mathbf{S} \tag{8}$$

By substituting $\mathbf{P}^T$ into the second equation, one gets

$$\mathbf{C}_t = \mathbf{T}_t\left(\mathbf{T}_c^T\mathbf{T}_c\right)^{-1}\mathbf{T}_c^T\mathbf{C}_c \tag{9}$$

Finally, considering the initial centring, the desired unknown concentrations are as follows:

$$\widetilde{\mathbf{C}}_t = \mathbf{T}_t\left(\mathbf{T}_c^T\mathbf{T}_c\right)^{-1}\mathbf{T}_c^T\mathbf{C}_c + \widetilde{\mathbf{E}}_t\,\mathbf{mean}(\widetilde{\mathbf{C}}_c) \tag{10}$$

The score matrices appearing in formula (10) can be readily found by multiplying both parts of Eqns (6) on the right by the loading matrix $\mathbf{P}$

$$\mathbf{P}^T\mathbf{P} = \mathbf{E} \Rightarrow \begin{bmatrix} \mathbf{T}_c = \mathbf{X}_c\mathbf{P} \\ \mathbf{T}_t = \mathbf{X}_t\mathbf{P} \end{bmatrix} \tag{11}$$

Expressions (11) correspond to the definition of scores, which are the projections of the centred initial data to the new principal component space. By solving the systems of matrix equations, one can also solve the inverse regression problem for other decompositions of initial data matrices.

Next we consider the application of multivariate calibrations in LIBS used for analysis of natural samples. Death *et al.*[110] carried out PCR-based quantitative analysis of iron and nickel ores from Australia and West Africa. The input spectral ranges were relatively narrow (24 – 50 nm) and the spectra were normalized to the total intensity. The authors did not perform cross-validation or use test sets of samples but restricted themselves to construction of cali-

bration models for various numbers of principal components (from 3 to 10). The relative prediction errors of the calibration models for the major components of iron ores were as follows: 4.8% for iron, 2.2% for aluminium and 3.7% for silicon. For some components, for example, for manganese or phosphorus, no good analytical results were obtained. Meanwhile, for nickel ores in which the iron content is twice lower and the phosphorus content is an order of magnitude higher (> 0.1 mass %) than in iron ores, the relative error of the calibration model for phosphorus was 5.5%. As a whole, the PCR allows rapid determination of the major components of ores with minimal pretreatment of spectral data.

Multivariate methods can be used not only to predict the chemical composition of the sample from spectral data but also to estimate some properties of the sample. Yaroshchuk *et al.*[165] used PLS regression of LIBS data to predict the loss on ignition in iron ores (0.2 mass % – 11 mass%). The measurements were carried out in air within the 385 – 855 nm range by an Echelle spectrometer (~ 0.08 nm resolution, 11000 channels — wavelengths). Ore powders pressed into pellets and natural materials without sample preparation were considered separately. The calibration model was constructed and tested using two independent sets of samples (~ 60 samples in each set). The minimum prediction error in the 10-fold cross-validation and the high value (> 95%) of explained residual variance[105] for the training data set justified the selection of twelve components for the regression model. Apart from the raw data, several types of data pretreatment were employed. The pretreatment included the detector background subtraction, background subtraction by the algorithm proposed by Gornushkin *et al.*,[166] normalization to the integral intensity of the spectrum or to the standard deviation. There, by the integral intensity was meant the sum of intensities at all wavelengths in the covered range. Normalization substantially improved the accuracy and reduced the root-mean-square error of prediction to 1.1 mass % both for pellets and the bulk ore samples.

During preparation to the Mars mission, scientists performed numerous investigations dealing with quantitative remote LIBS analysis of minerals in the simulated Martian atmosphere.[26] For example, by using PLS1 regression, the contents of the major components of phyllosilicates and igneous rocks, Si, Al, Ti, Fe, Mg, Mn, Ca, K, Na and P, were determined with an average prediction error of 7%, 4%, 38%, 15%, 14%, 70%, 11%, 35%, 48% and 38%, respectively.[167] These data were not given in the original publication but we obtained them as the ratio of the root-mean-square error of prediction of concentrations for the test set to the average concentration for all 117 samples of phyllosilicates and igneous rocks.

Wiens *et al.*[168] proposed an algorithm for initial data processing and pre-flight calibration of the instrument in relation to 69 rock standards — carbonates, sulfates, phyllosilicates and so on. Our estimates of the relative prediction errors of PLS regression for Si, Ti, Al, Fe, Mn, Mg, Ca, Na and K were 17%, 81%, 38%, 65%, 14%, 49%, 48%, 43% and 57%, respectively. The large errors may be due to inclusion of all samples into a single calibration model without considering the matrix effects of various rocks. Ollila[169] reported the first semiquantitative estimates of the contents of trace components (Rb, Li, Sr, Ba) in six samples from the Martian surface obtained by the LIBS instrument ChemCam mounted on the Mars rover. The contents were determined using both the PLS regression and univariate calibrations based on integral intensities of analytical lines. Although the errors were high, the same results were achieved for both procedures. The contents (c) of the following elements were determined:

Element	Li	Ba	Rb	Sr
c (mass %)	0.001 – 0.006	0.1	0.01	0.1

Recently, German and Czech research groups published a joint paper[111] in which they proposed an approach to decreasing the matrix effects and improving the accuracy of the analysis with preliminary sample classification prior to calibration. This implies splitting of samples into groups and separate calibration for each group. This approach was tested in relation to 27 copper ore powders (copper content of 0.06 mass % – 0.79 mass %) on an adhesive tape surface. After removal of outliers, the spectra were normalized to the total intensity and averaged. The univariate calibration against the integral intensity of the copper line at 521.8 nm without preliminary splitting of samples into groups was found to be unsuitable for solving analytical problems ($R^2 \approx 0.23$ and 0.5 for different LIBS systems). When the samples were divided into groups according to the type of rock (andesite, diorite, monzonite) identified by experienced geologists, calibrations became better ($R^2 \approx 0.57 - 0.87$) but the accuracy still remained moderate; for some samples, pronounced deviations are observed.

Multivariate calibration models were also constructed for the whole set of samples; in this case, the intensities of the fifteen matrix lines (Al, Si, Na, Ca) and four copper lines (including the resonance lines at 324.75 and 327.39 nm) served as the input data. It was noted[111] that copper lines were not self-absorbed; therefore, the application of linear regression procedures was considered justified. However, this statement casts some doubt, because we observed[170] self-absorption of these resonance lines in analysis of soils with a copper content of > 0.008 mass %. The results of PCR and PLSR leave-one-out cross-validations with 3 – 5 principal components demonstrated improved predictive ability (the R^2 value for a set of predicted and reference concentrations reached 0.79). However, this is insufficient for accurate analysis; therefore, an attempt was made to divide samples into groups using the spectral data, *i.e.*, based on the chemical composition of the sample matrix. The PCA score analysis and data clusterization according to the Gauss algorithm in the principal component space were used to find outliers for each class. Some samples were misclassified by geologists as certain types of rocks. Moreover, splitting of the samples into the phyllite and potassium groups is demonstrated. Partial calibrations were constructed using reduced sets of each type of samples from the potassium group. The final result of prediction of copper concentrations in potassium group samples has substantially improved to $R^2 = 0.95$ for the set of reference and predicted concentrations.

IV.3. Calibrtion-free quantitative analysis

Ciucci *et al.*[171] proposed a calibration-free LIBS technique (CF – LIBS), which does not require reference samples but uses only spectral information and atomic line parameters. Calculation of the composition by this method requires that three conditions be met: the absence of self-absorption, the

presence of a local thermodynamic equilibrium and the same proportions of the elements in the sample and in the plasma. Briefly, the essence of the method is as follows: all values that refer to transition parameters in Eqn (4), which describes the line intensity, are moved to one side of the equation and then the logarithm of both sides is taken

$$\ln\left(\frac{4\pi\lambda I}{hcgA}\right) = -\frac{E}{kT} + \ln\left(fn\frac{1}{Z(T)}\right) \tag{12}$$

Then the left-hand side of Eqn (12) with the use of atomic spectral lines of one element and, individually, the lines of its each ionic species was plotted against the energy of the upper level. The plots thus obtained are usually called Boltzmann plots. The slope of the straight line can serve to determine the temperature, while the y-axis intercept b can be used to find the number of element species occurring in a particular ionic state

$$b = \ln\left(fn\frac{1}{Z(T)}\right) \Rightarrow n = \frac{e^b Z(T)}{f} \tag{13}$$

After calculation of the number of species n_i taking account of all ionization states j for all k elements, it is possible to exclude the experimental parameter f and determine the fraction (ω_i) of each element in the plasma

$$\omega_i = \frac{n_i}{\sum\limits_{i=1}^{k} n_i} = \frac{\sum\limits_{j=1}^{m_k} e^{b_i^{(j)}} Z_i^{(j)}(T)}{\sum\limits_{i=1}^{k}\sum\limits_{j=1}^{m_k} e^{b_i^{(j)}} Z_i^{(j)}(T)} \tag{14}$$

The calculations are often restricted to only atomic lines, which may give rise to large errors of analysis in the case of high content of ions in the plasma.

Despite the numerous advantages of this approach, its practical implementation is difficult for several reasons, first of all, due to the effect of self-absorption and great uncertainties of the known Einstein coefficients for many lines. Therefore, the methods for detecting and correcting the self-absorption as well as instrumental methods aimed at generation of more homogeneous plasma are being actively developed.[172] Nevertheless, currently CF-LIBS provides, most often, semiquantitative determination of the major and minor components of soils, ores and minerals, which is suitable for the preliminary sample classification. For increasing the trueness of determination, a 'hybrid' technique was proposed that employs an additional synthetic sample similar in composition to the analyte sample. This technique was applied to classify emeralds in terms of the provenance [173] and to determine lead in soils.[174]

For independent calculation of the experimental parameter f and possible deviations from the local thermodynamic equilibrium, it was proposed to use certified reference materials.[4] Although this approach ensures some increase in the trueness, it is of restricted use due to the required fairly complicated measurements on plasma diagnostics, while the use of traditional calibration is possible. De Giacomo [175] proposed an interesting procedure for determination of the composition of metallic meteorites by fundamental characteristics. The contents of components were calculated from the rate of decay of plasma spectrum lines and collisional excitation cross-sections. A CF-LIBS procedure for estimating the contents of major components in meteorites and in some minerals has been proposed;[176 – 178] according to this method, the concentration of the major component is determined from the stoichiometry of the sample matrix (*e.g.*, aluminium in alexandrite) and is used in the denominator of formula (14), *i.e.*, the content of trace components is calculated as the ratio to the aluminium content. This approach proved to be especially efficient when it is necessary to study the spatial distribution of trace components in the sample.

IV.4. Methods for increasing the sensitivity

The background contents of many elements in soils do not exceed 10 – 100 ppm and for some scattered elements (for example, gold), the content can be a few ppb.[179] In sea and river water, the background contents are usually 2 – 3 orders of magnitude lower than in soils (< 100 μg litre^{-1}).[180] The occupational exposure limits (OEL) of toxic elements (Pb, Hg and so on) in natural media [181, 182] are determined proceeding from the background contents; therefore, OEL are usually somewhat higher than the background. For environmental monitoring of soil and water contamination and for exploration activity, the sensitivity of analytical methods should be sufficient for quantitative analysis at the background concentration levels of elements.

In analytical practice, the term 'sensitivity' implies the change in the analytical signal upon a specified change in the content, or the first derivative of the calibration function with respect to the analyte content.[183] The dimensionality of this quantity is determined by conditions of the particular measuring system; therefore, we will compare the potentials of methods or procedures in terms of the limits of detection ($c_{\min}$) of components. At a local thermodynamic equilibrium and optically thin plasma, the relationship between the emission line intensity I and the number of analyte species (N_a) in unit volume of the plasma is specified by Eqn (4). In the general case, N_a is a function of temperature T, plasma electron density n_e and the degree of atomization α. Since the key plasma parameters are dependent on time t, the experimentally observed line intensity is an integrated quantity from the instant when radiation collection starts τ (delay time) to the instant of $\tau + \delta\tau$ ($\delta\tau$ is the gate width). Thus, in the general form, the LIBS limit of detection can be written in the following way

$$c_{\min} = \frac{3\sqrt{s_d^2 + s_b^2}}{FAg}\left[\int_{\tau}^{\tau+\delta\tau} \frac{N_a(t)}{Z(t)} \exp\left(-\frac{E}{kT(t)}\right) dt\right]^{-1} \tag{15}$$

where s_d and s_b are the standard deviations of the signal caused by the detector and the plasma background, respectively; F is some parameter including f. In order to decrease $c_{\min}$, it is necessary to

— collect as much radiation as possible (maximize F);

— choose analytical lines with the maximum product Ag;

— decrease the detector noise s_d;

— optimize the selection of temporal parameters τ and $\delta\tau$ in order to decrease s_b, while the signal to noise ratio should be maximized;

— increase the number of emitting species by either more efficient ablation or additional excitation of analyte atoms;

— increase the plasma lifetime.

Below we consider the publications devoted to enhancement of the sensitivity of LIBS for determination of traces in environmental samples according to the approaches listed above.

IV.4.a. Selection of the analyte species

According to the IUPAC recommendations,[184] analyte species means the chemical form of the analyte that directly generates the analytical response of the measuring system. Most often, the species used in LIBS are the analyte atoms, because the content of atoms is maximum at typical laser plasma temperatures (0.5 – 2 eV) and electron densities (10^{16} – 10^{18} cm^{-3}).[44] For determination of elements that are highly ionized in plasma (as a rule, $E_{ion} < 10$ eV), singly charged ions are the best species if the excitation potentials of these ions are relatively low (1 – 5 eV). First of all, this refers to alkaline earth metals. Singly charged ions can serve as analyte species for some transition metals.

It is noteworthy that neutral atoms are the species of choice for determining alkali metals, despite their low ionization potentials. This is caused by high excitation potentials of the singly charged ions of these metals. For example, the energy of the first excitation state of sodium ion Na II $^3P_2^\circ$ is ~ 33 eV;[185] therefore, the fraction of the excited sodium ions in the plasma is negligibly low even at a temperature of 2 eV.

Apart from atoms and singly and doubly charged ions, bands for the violet CN system, C_2 Swan system, AlO, TiO, OH and CH[186] and even bands for C_3 molecules[187] are often observed in air. Recently, Gaft *et al.*[11] proposed using the CaF and CaCl molecules instead of atoms as the analyte species for determination of fluorine and chlorine in rocks due to their high excitation (> 10 V) and ionization (> 12 eV) potentials and $\alpha \ll 1$. In the presence of a low-intensity atomic line of fluorine in the spectrum, this provided semiquantitative estimation of its content in Martian rocks at the site of landing of the Curiosity rover. Niki *et al.*[188] proposed using the molecular bands of the monoxide BO for determining the ^{10}B and ^{11}B isotopes with allowance for an significant isotope shift (~ 0.5 nm). While developing this area, Russo *et al.*[189] demonstrated simultaneous determination of ^{10}B and ^{11}B isotopes based on the BO bands (0.5 – 8 nm shift),[190] simultaneous determination of the ^{86}Sr, ^{87}Sr and ^{88}Sr isotopes based on the strontium monoxide (0.05 – 0.25 nm shift), monofluoride (~ 0.05 nm shift) and monochloride (~ 0.1 nm shift),[191] and determination of ^{12}C and ^{13}C isotopes based on the C_2 and CN molecular bands (~ 0.8 nm).[192]

The choice of analytical lines for attaining high sensitivity is usually governed by the following key principles:

— it is better to choose transitions to the ground level (*i.e.*, resonance lines) if it is possible under conditions of analysis; for example, the resonance lines of many nonmetals lie in the vacuum UV region (for chlorine, Cl I 134.72 nm) and, hence, they are unsuitable for analysis in air or in a CO_2 or nitrogen atmosphere;

— among the most intense lines of the given species, one should select the line with the maximum product of the transition probability A by the statistical weight g of the upper level; indeed, out of the two components of the copper resonance doublet, 324.75 and 327.40 nm, with similar transition probabilities [$A = 1.37 \times 10^8$ s^{-1} (see Ref. 193)], the former line is more sensitive because the statistical weights of the upper states of these transitions are related as 4 : 2;

— lines that are located in the region of the highest detector sensitivity should be selected; for example, the nonresonance Pb I line at 405.78 nm, which is comparable in intensity with the resonance Pb I line at 283.30 nm, is very popular for determination of lead in soils and waters owing to higher sensitivity of many of detectors in the 400 – 500 nm range;

— the spectral interferences from intense and medium-intensity lines of major components should be minimal; since the iron content in soils, rocks and ores is, on average, $\sim 5\%$ (Ref. 179), the main interfering components in the analysis of these materials are iron atomic and ionic lines (as an example, the selection[170] of the analytical line among several multiplets for determination of molybdenum in ores and soils can be mentioned).

IV.4.b. Double-pulse and multi-pulse plasma excitation

In the practice of LIBS analysis, the number of excited species is increased by using additional impact on the plasma by the second laser pulse which is delayed with respect to the ablation pulse by 100 ns – 100 μs. Initially, Cremers *et al.*[194] proposed using the second laser pulse for analysis of aqueous solutions. Plasma expansion in water induces pronounced collisional deactivation of excited atoms; therefore, the emission is much lower than in air. The first pulse forms a bubble in the liquid bulk, while the second pulse ignites plasma in the bubble at the interface. This design substantially improved the precision of determinations and decreased the limits of detection of boron and beryllium to 10 – 100 ppb. To increase the mass of the ablated sample, Bukharov and Pershin[195] proposed the generation of two successive pulses on one active element with a 40 μs delay. Later, Yamamoto *et al.*[196] were able to decrease the limits of detection of many toxic metals in soils 2 – 5-fold by means of the multi-pulse version of LIBS in which the delays between five to seven successive pulses were ~ 20 μs. As the key causes for the intensity growth, the increase in the following parameters is considered:

— the ablated sample mass;

— plasma temperature;

— plasma lifetime;

— plasma volume.

Depending on the geometric configuration of the optical path of the laser beams, three types of double-pulse LIBS are distinguished. In the collinear scheme (see Fig. 5 *b*), both pulses move along the same optical path or at a small angle (most often, not more than 5°) relative to each other. Since this design is implemented most easily, in particular, for remote measurements, it is used by authors of $\sim 3/4$ of the total number of studies devoted to double-pulse LIBS. In the orthogonal design (see Fig. 5 *c*), the optical paths of the two pulses are perpendicular to each other. Two sorts of this system are known:

— with plasma re-heating: the first pulse orthogonal to the sample surface ablates the substance, while the second pulse is absorbed by the plasma, and hence the plasma temperature rises;

— with pre-ablation: the first pulse parallel to the surface creates the necessary rarefaction above the ablation area, while the second pulse induces ablation of the sample material to the rarefied space.

Gautier *et al.*[197] discovered the correlation between the factor of enhancement of the emission signal in the orthogonal configuration and the excitation potential of the transition: the higher the excitation potential, the greater the enhancement. Considering the increase in the ablated sample mass, plasma homogeneity and duration of the emission, Tognoni and Cristoforetti concluded in a review[198] that the orthogonal pre-ablation configuration is preferred for determination of trace components. Obviously, the practical implementation of the orthogonal configuration is more complicated, as this requires an additional optical path; in some cases, it cannot be implemented at all. Detailed comparative analysis of the effects of wavelength, energy, pulse duration and the delay between the pulses on the analytical signal was carried out in several reviews devoted to the potential of double-pulse LIBS[45, 198–201] and in a monograph.[32]

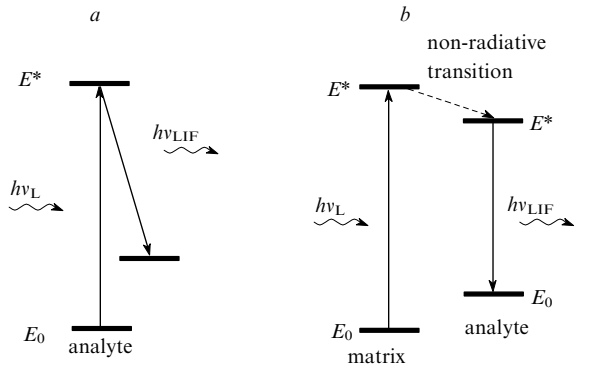


Figure 9. Diagrams of additional resonance excitation of analyte (*a*) and sample matrix (*b*) atoms in LIBS.

IV.4.c. Additional resonance excitation

The number of excited species of the element to be analyzed in the plasma can be increased by means of an additional tuneable source of radiation, which allows almost complete transition of atoms from the ground to excited state. Two methods for the enhancement of atomic emission have been proposed. One method is based on the resonance excitation of analyte atoms and subsequent recording of their fluorescence simultaneously with the emission spectrum of the plasma (Fig. 9 *a*). As a rule, transition with the highest Einstein coefficient is utilized as the fluorescent transition. In essence, this is a usual combination of laser-induced fluorescence (LIF) and laser ablation proposed for the first time by Kwong and Measures[202] and described in detail in several reviews.[203–205] In this case, the selectivity is higher than in the conventional LIBS due to the absence of spectral interferences from major components, especially, those having large numbers of lines, for example, iron or tungsten.

The instrumental implementation of LIFS–LIBS (LIFS is LIF spectroscopy) is possible by the use of tuneable dye lasers, diode lasers and, more recently, optical parametric oscillators. Usually, the time delay between the pulses of the ablation and excitation lasers is chosen to be from 1 to 50 μs with the goal to reach the maximum population of the ground state of analyte atoms. In the case of such delay, the background plasma emission and the intensity of emission lines of other sample components are much lower. Apart from the analytical line, other lines of the analyte will also be enhanced.

Telle *et al.*[206] observed enhancement of aluminium lines at 309 nm and a doublet component at 394.40 nm upon excitation of the aluminium resonance line at 396.15 nm with a tuneable dye laser. Ezhov *et al.*[207] succeeded in lead determination in granites at a few ppm level by using additional excitation. A combination of LIFS and LIBS was utilized[208] to monitor the quality of marble purification based on enhancement of very weak aluminium lines, while in another publication,[209] a considerable increase in the sensitivity of cadmium and thallium determination in soils (down to 0.5 ppm) was demonstrated. Koch *et al.*[210] employed the LIFS of indium for its determination under water at a level of tens of ppm; this was done using a double-pulse collinear LIBS configuration for creating a bubble in the liquid and subsequent ablation in the vapour. A flow-type LIFS–LIBS design for lead determination in water at 0.1 ppm level was developed by Fedosejev's[211] and Sabsabi's[212] research groups. Since fluorescence of only one element can be observed at a specified excitation frequency, this combination of methods suffers from a considerable drawback being a single-element analysis. Meanwhile, owing to the narrow line of generation of excitation sources (< 1 pm), it is possible to study the isotope composition of the sample. For instance, Smith *et al.*[213] determined the isotope composition of uranium ore [isotope shift $\lambda(^{235}\mathrm{U}) - \lambda(^{238}\mathrm{U}) = -17.7$ pm] up to the ratio $^{238}\mathrm{U}/^{235}\mathrm{U} \approx 2000$, the limit of detection of $^{235}\mathrm{U}$ in ore being 100 ppm.[214]

Note that LIBS analysis requires both a high resolving power of the spectrograph and conditions minimizing line broadening caused by the Stark effect because of small isotopic shift. Cremers and co-workers[215, 216] determined plutonium, uranium and lithium isotopes by means of a compact Echelle spectrometer with a resolving power of 75 000 at the levels of natural abundances of the isotopes (0.7 mass % $^{235}\mathrm{U}$ and 7.5 mass % $^{6}\mathrm{Li}$).

To overcome the single-element limitation, Lui and Cheung[217] proposed a different configuration involving resonance excitation of atoms of the major component of the analyte. Excess internal energy is transmitted *via* collisions to all laser plasma atoms (Fig. 9 *b*), thus enhancing the emission lines in the spectrum. Apart from the excitation of atoms of all elements present in the sample, owing to the great number of atoms of the major component, the efficiency of the resonance pumping of the plasma increases. As a result, the intensity of many analytical lines increases more than 100-fold without excitation frequency tuning, which also reduces the time of analysis.[218] The loss of instrumental simplicity upon combination of LIFS and LIBS due to an additional source of coherent and monochromatic radiation is the key drawback of this approach to increasing the sensitivity, especially for *in situ* analysis. Moreover, the cost of this source exceeds in some cases the cost of ICCD, which also restricts the laboratory use of fluorescence for determining traces of elements in soils, ores and waters.

IV.4.d. Additional excitation in a spark discharge

The cross spark discharge excitation of the relatively cold cloud of species vaporized by laser radiation was proposed by Brech and Cross.[219] The spark was formed between two

electrodes, located 2 – 5 mm above the sample surface, after the substance had been ablated into the space between the electrodes. This way of increasing the sensitivity was fairly popular in laser spark spectrometers with photographic detectors (Carl Zeiss, Jarrell-Ash, LOMO and so on) in the 1960s – 1980s. The advantages of this approach include

— increase in the plasma lifetime to 0.1 – 10 ms and, as a consequence, enhancement of the emission;

— decrease in the continuous background radiation of the laser plasma;

— possibility of trace analysis for non-conducting materials (*e.g.*, soils, sands and so on), unlike the traditional spark emission analysis.[127]

The key problem associated with the use of this approach is rather low precision [RSD of 25% to 40% (Ref. 220)] resulting from the high potential drop between the electrodes (up to several kilovolts). The interest in this method declined after the appearance of multichannel ICCD in analytical practice. However, spark excitation is still considered to be a highly sensitive alternative to systems with intensifiers due to high cost of these detectors. For example, a Russian patent was granted [221] claiming a laser spark system for determining zinc and beryllium in soils at the background levels (1 – 10 ppm). As the detector, this system employs a relatively inexpensive CCD device manufactured by MORS (Russia). More recently, Skripkin and co-workers [222] demonstrated the applicability of this system for monitoring the heavy metal and arsenic contamination of Moscow city soils. The researchers from the Institute of Physics, National Academy of Sciences of Belarus, tested a combination of a cross spark discharge with laser ablation for determining the total content of C in soils.[13] It was shown that the sensitivities of carbon determination by this method and by double-pulse collinear ablation are comparable.[223] The combination of LIBS with additional spark excitation has attracted attention of Chinese researchers due to the low cost of such system. A tenfold enhancement of lead and arsenic analytical lines in the spectra of soils were reported.[224, 225] The sensitivity ($\sim$19 ppm for Pb and $\sim$9 ppm for As) proved to be only little better than in the case of conventional LIBS.

One more design involving cross spark discharge in which the sample serves as the second electrode was proposed by Chen *et al.*[226] It is evident that this design is possible only for current-conducting materials (metals, alloys, *etc.*). Furthermore, the variations of the spark position on the sample surface deteriorate repeatability of the results. Despite these substantial drawbacks, the following advantages should be noted: first, the luminous zone in the discharge becomes larger due to the increase in the electrode (sample) surface; second, initiation of the discharge channel requires a lower potential drop ($\sim$200 – 300 V) due to the presence of laser-induced charges. Moreover, by preliminary electrodeposition of mercury on the surface of pure copper, extremely high sensitivity of Hg determination (2 ppb limit of detection) in water was achieved.

Thus, despite the relatively low cost of the high-voltage system compared to the system involving a second laser or intensifier, the use of cross spark discharge has the following basic drawbacks:

— contaminations introduced from the electrode materials considerably deteriorate the accuracy of analytical measurements and the selectivity — spectral interferences arise due to the lines of major components of the electrode material;

— the short distance between the discharge gap and the sample surface precludes direct analysis of liquids and remote monitoring of hazardous objects such as radioactive and poisonous materials.

In view of these drawbacks, one should not expect much interest in the development of this approach.

IV.4.e. Additional microwave excitation

One more approach to increasing the laser plasma lifetime was proposed by Niemax and co-workers.[227] A microwave field was used; in the absence of laser plasma, the microwave field is unperturbed, while the charged species coming from the laser plasma induced a discharge in the microwave field, resulting in the formation of long-lived plasma with intense emission. The lifetime of microwave plasma is 1 – 10 ms, which is three orders of magnitude longer than the laser plasma lifetime. The obvious advantages of the microwave plasma include the lack of necessity of sample conductivity and the low-intensity plasma background caused by low electron density. Another important advantage, *i.e.* there is no interaction between the microwave plasma and the sample, accounts for the substantial decrease in the matrix effect. The optimal argon pressure for microwave excitation was found to be $\sim$10 kPa. Using a microwave system, Niemax and co-workers [228] achieved an unprecedented limit of detection for sodium in quartz — 40 ppt.

Liu *et al.*[229] estimated the potential of microwave plasma generated in air. Unlike the double-pulse LIBS, in the case of the microwave field-induced increase in intensity, the lower the line excitation potential, the higher the intensity increase. Although the copper and silver resonance lines were enhanced $\sim$23-fold, the limits of detection of these elements in soils proved to be considerably higher than the average abundance of the elements.[230] For miniaturization and elimination of the necessity of using a special microwave chamber, Tampo *et al.*[231] simplified this approach by placing an antenna (metallic ring) at a short distance from the sample for microwave discharge ignition. Nevertheless, the necessity to use a power supply unit for the magnetron generating the microwave field and the presence of contact space for maintaining the microwave discharge still restrict the feasibility of remote analysis. Therefore, currently this approach is not widely used.

IV.4.f. Plasma confinement in an external magnetic field

Since laser-induced plasma contains a multitude of moving charged species (ions and electrons), an external magnetic field affects its expansion rate; moreover, plasma resists the propagation of magnetic field inside itself. While investigating hydrodynamic stability of plasma, Bhadra [232] ascertained that in a steady magnetic field with the induction B, plasma expansion is completely terminated at the distance $r \sim B^{-2/3}$. For comparison of the plasma expansion velocities in the absence (v_1) and in the presence (v_2) of a magnetic field, Rai *et al.*[233] proposed a dimensionless parameter β

$$\beta = \frac{8\pi NkT}{B^2} \qquad (16)$$

where N is the number of charged particles in the plasma. In essence, this parameter expresses the ratio of the kinetic energy of charged species to the magnetic field energy; therefore, for high β values (*i.e.*, weak field), the plasma expansion velocity will not change, while for small β (*i.e.*, very strong field) plasma deceleration will be efficient

$$\frac{v_2}{v_1} = \sqrt{1 - \frac{1}{\beta}} \qquad (17)$$

Since the magnetic field does not interact with the electrons or ions that move along the lines of force or at a small angle to these lines, plasma will be extended along the axis perpendicular to the lines of force.[234] The parameter β can be used for qualitative description of the evolution of plasma interaction with the external field and the evolution of the LIBS signal intensity. In the extreme case, where the plasma kinetic energy is equal to the magnetic field energy density ($\beta = 1$), the velocity of an assembly of charged particles will turn to zero. In this instant, the number of collisions in the plasma and, hence, the number of excited atoms increase. Therefore, the intensity evolution curves have one or two peaks corresponding to deceleration of relatively fast electrons and slow ions, as was demonstrated by Shen *et al.*[234] The positions and amplitudes of these peaks virtually do not depend on the laser beam energy but with an increase in B, the peak will shift toward short delays. The competition of the collisional and radiative deactivations of excited states would result in different magnetic field effects on the atomic and ionic analyte lines in the spectra. Using the principal component method, a number of factors affecting the enhancement of intensity in a magnetic field have been defined.[235] A negative correlation between the signal enhancement and the first ionization potential was identified for atoms; a strong positive correlation between the signal enhancement and the sum of the first ionization potential with the element – oxygen bond energy was found for ions.

There are few papers on the application of the external magnetic field to determine traces of elements. A number of papers [233, 236] devoted to determination of some metals in a water jet can be mentioned. Despite the high-strength magnetic field ($\sim$5 kG) applied to the plasma, the limits of detection of Mg, Ti, Cr and Mn were improved only $\sim$1.5-fold (down to hundreds of ppb). The lack of interest in the use of the magnetic field for increasing the LIBS sensitivity is due to the following reasons:

— spectral line broadening and even displacement due to the Zeeman effect can deteriorate the trueness of analysis: an increase in the field strength, which is expected to enhance the magnetic plasma confinement, would additionally increase the errors *via* more pronounced multiplet splitting;

— due to considerable inhomogeneity of the magnetic field [237] caused by expansion of the small-size plasma, precision of the results would be considerably impaired;

— minor increase in the sensitivity of this approach does not counterbalance the impairment of accuracy;

— the addition of new parts (permanent magnets or electromagnets and synchronization and power supply units) seems unnecessary for analysis of environmental samples *in situ*.

IV.4.g. Plasma compression by shock wave in a microchamber

One more method for confinement of the laser plasma is to restrict propagation of the the plasma front. The formation and expansion of the laser-induced plasma in condensed media is known to be accompanied by shock wave formation. If some barrier (*e.g.*, a plate) is placed on the shock wave propagation route, the wave is reflected towards the plasma front. As a result of the collision, the temperature in the plasma front rises and the number of excited species and the emission signal intensity increase. The sequence of processes that are involved in the plasma confinement in a chamber is depicted in Fig. 10. Since the shock wave energy density decreases with distance as $\sim 1/r^2$, the distance between the barrier and the ablation spot should be short.

Popov *et al.*[238] proposed a cylindrical microchamber 4 mm in diameter with a small hole for the laser radiation and a hole for observing plasma emission. The application of this chamber for analysis of highly contaminated soils made it possible to decrease the limits of detection of some toxic elements (mercury, arsenic, lead, *etc.*) by factors of $\sim$3 – 5.[239] More effective reflection should be expected from the walls of a hemispherical chamber due to the spherical symmetry of the shock wave. Thus, Guo *et al.*[240] observed more than a 12-fold increase in the intensity of lines of minor components by using a hemispherical chamber. A chamber of this type can function as an integrating sphere due to the reflection of plasma radiation by the chamber walls. Chen *et al.*[241] demonstrated a twofold increase in the intensity of barium lines in a study of soils using a flat mirror mounted in the vicinity ($\sim$10 mm) of the plasma.

By analogy with the double-pulse excitation, the enhancement of the emission signal upon the compression of plasma by the shock wave is specific to each element and its spectral lines. Indeed, Li *et al.*[242] found that the higher the excitation potential of the analyte line, the more pronounced the effect; this is especially useful in the case of non-metals with high excitation potentials ($>$7 eV). The simple design of this chamber is combined with the possibility of the simultaneous use of other intensity enhancement methods — collinear double-pulse ablation,[243] confinement in a steady magnetic field [244] or additional spark discharge excitation.[245] The main problem faced by analytical application of this chamber is deterioration of repeatability of the results (2 – 3-fold) due to the breakdown on aerosol particles that remain in the chamber after the previous laser shots. To solve this problem, it was proposed [246] to purge the chamber with air, and this provided a $\sim$5-fold decrease in the RSD. Owing to compactness and compatibility with various instruments and high sensitivity, the use of such a microchamber in the field appears fairly promising.

IV.4.h. Figures of merit

The sensitivity of determination of a chosen element in LIBS depends on particular experimental conditions. The detection limits of elements in environmental samples are presented in numerous publications (see, for example, Refs 247 – 299). The data for most common elements are summarized in Table 2 with indication of conditions of analysis. The number of publications containing data on LIBS sensitivity for real natural and industry-produced waters is moderate; therefore, data on the sensitivity of determination in pure aqueous solutions are also given. The second column presents the analytical line of the element in

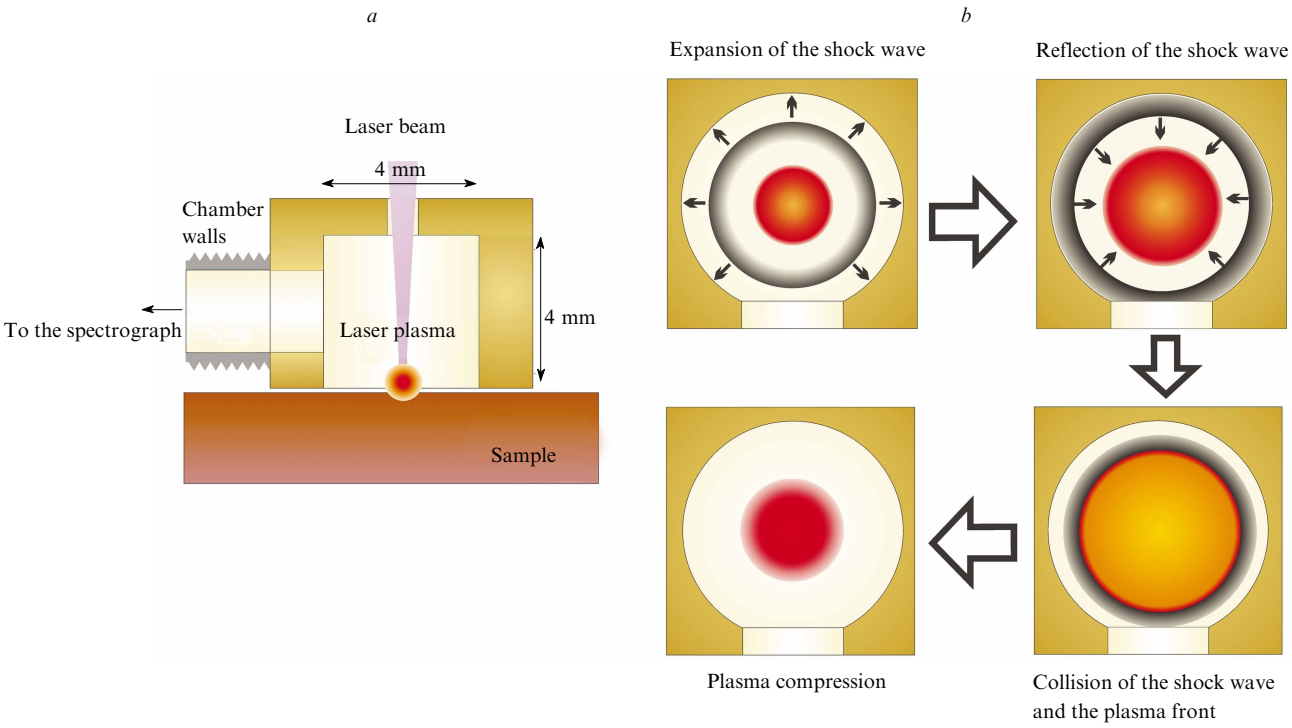


Figure 10. Microchamber for LIBS measurements (*a*) and the diagram illustrating its operation principle (*b*).

accordance with the accepted spectroscopic designation of the species [247] and the corresponding wavelength in nanometres taken from known spectral line databases.[84, 85, 248] The results of studies in which the analytical line wavelength is not reported or this line could not be correlated with the database value are not given. In the case where authors could not resolve the doublet or multiplet structure of the analytical line due to poor resolution, the wavelengths of these line given in the Table are rounded to units. The limits of detection for solids (wood, ores, soils, minerals and so on) are given in ppm and for liquids they are in milligrammes per litre.

The brief description of the conditions of analysis is given in the following notation: specific conditions//atmosphere//laser system characteristics//detector type. The possible specific conditions include the application of microwave plasma (MWP), spark discharge (S), spatial confinement in a microchamber (SC), electrodeposition (ED), extraction (Ex), preconcentration of elements (PC) or element hydrides (HG), ablation in a jet (Jet) or liquid bulk (Liq), aerosol breakdown (AD); some parameters describing these conditions can be indicated after the slash. The absence of such designations implies that the plasma is formed on the surface of a solid or liquid sample. If ablation occurs in an atmosphere other than air, gases or gas mixtures in which plasma is formed are indicated; after the slash, the gas or liquid pressure in Pascals is given if it differs from the atmospheric pressure.

Seven types of lasers used in the studies are designated in the following way: L_1 is the Nd:YAG laser, L_2 is the CO_2 laser, L_3 is the XeCl laser, L_4 is the Ti: sapphire laser, L_5 is the dye laser, L_6 is the ArF laser and L_7 is optical parametric oscillator. If two or more lasers are used in the study, their types as well as parameters are listed with the plus sign. When the same laser is used to generate several pulses (with either one or two crystals), only one laser type is indicated. The laser parameters are listed one by one and separated by slashes. The following parameters are indicated: wavelength (λ/nm), energy (E/mJ), power density (W/GW cm^{-2}), fluence (F/J cm^{-2}), pulse duration for femtosecond lasers (τ/fs), pulse delay (Δ/μs) for double- and multi-pulse LIBS designs; double-pulse configuration: cc is the collinear configuration, oc is the orthogonal configuration. When some parameter is not indicated in the original publication, this parameter is omitted in the notation. The detectors are designated in the following way: D_1 is the ICCD, D_2 is the PMT, D_3 is the intensified linear photodiode array, D_4 is the CCD. As in all emission spectral methods, the important figure of merit such as the linear dynamic range is limited in LIBS from above by self-absorption. For most lines presented in Table 2, the dynamic range is $3 \times c_{min} - 1000 \times c_{min}$ and does not exceed two to three orders of magnitude. If it is necessary to analyze samples with high analyte contents, non-resonance lines should be chosen.[170] The relative standard deviation within the linear dynamic range is usually 5% – 25%.

Generally, the limits of detection for soils, ores, rocks, coals and minerals are in the range of 1 – 100 ppm; for easy-to-excite and easy-to-atomize elements, the limits are very low, for example, for beryllium, it is <1 ppm, whereas elements that are hard to excite and atomize (*e.g.*, fluorine) have relatively high limits of detection.

Currently, the sensitivity of LIBS is, on average, lower than the sensitivity of LA – ICP – AES or LA – ICP – MS, but for many elements, it is higher than the sensitivity of X-ray fluorescence spectrometry. Using LIBS, it is possible to perform the environmental monitoring of the overall soil contamination by metals such as lead, zinc, beryllium and

Table 2. Achieved limits of detection of elements in environmental samples (ppm/mg litre^{-1}).

Line	c_{min}	Conditions	Line	c_{min}	Conditions
Wood [249]			Soils, sands and so on.[13, 170, 209, 239, 255 – 259, 264 – 267]		
Al I 394.40	3.3	$L_1/\lambda1064/E70//D_1$	Al I 309.20	190	$CO_2/700//L_1/\lambda1064/E40//D_1$
As I 234.98	2.7	$L_1/\lambda1064/E70//D_1$	Ba II 455.39	15	$CO_2/700//L_1/\lambda1064/E40//D_1$
B I 249.77	0.3	$L_1/\lambda1064/E70//D_1$	Fe I 404.58	490	$CO_2/700//L_1/\lambda1064/E40//D_1$
Cr II 283.56	< 1	$L_1/\lambda1064/E70//D_1$	K I 769.89	550	$CO_2/700//L_1/\lambda1064/E40//D_1$
Cu I 324.75	0.3	$L_1/\lambda1064/E70//D_1$	Na I 588.99	10	$CO_2/700//L_1/\lambda1064/E40//D_1$
Pb I 280.20	0.7	$L_1/\lambda1064/E70//D_1$	Rb I 780.03	20	$CO_2/700//L_1/\lambda1064/E40//D_1$
Si I 288.16	1	$L_1/\lambda1064/E70//D_1$	Ti II 334.9	30	$CO_2/700//L_1/\lambda1064/E40//D_1$
Sn I 286.33	2.2	$L_1/\lambda1064/E70//D_1$	Be II 310.04	0.4	$L_1/\lambda1064/E186//D_3$
			Mn I 403.45	6.7	$L_1/\lambda1064/E186//D_3$
Ores, rocks [170, 250 – 254]			C I 833.51	700	$S/1\ \mu F/4\ kV//L_1/\lambda1064/E180//D_4$
Ag I 328.07	0.3	$L_1/\lambda355/E21//D_1$	Co I 399.53	1	$L_3 + L_5/\lambda308 + 352.98/W1/\Delta16/oc//D_2$
Pb I 405.78	8	$L_1/\lambda355/E21//D_1$	Hg I 435.83	25	$SC//L_1/\lambda1064/E450//D_4$
Ca I 431.86	30	$L_3/\lambda308/E40//D_2$	V I 437.92	1	$SC//L_1/\lambda1064/E450//D_4$
Mg I 518.36	230	$L_3/\lambda308/E40//D_2$	Pb I 405.78	1	$L_1/\lambda1064//D_3$
Si I 390.55	1500	$L_3/\lambda308/E40//D_2$	As I 234.98	3.3	$L_1/\lambda1064/E450//D_2$
Ti I 498.17	230	$L_3/\lambda308/E40//D_2$	Cr I 425.43	2.5	$L_1/\lambda1064/E450//D_2$
F I 685.60	135	$He//L_1/\lambda213//D_1$	Ni II 231.60	6.8	$L_1/\lambda1064/E450//D_2$
Mn I 403.07	10	$L_1/\lambda532/E30//D_3$	Zn I 213.86	18	$L_1/\lambda355/E50//D_1$
P I 214.91	10	$L_1/\lambda532 + 532/E140 + 140/\Delta0.5/cc//D_4$	Cu I 324.75	0.6	$L_1/\lambda355/E21//D_1$
U I 356.66	150	$L_1/\lambda532/E10//D_1$	Mo I 313.26	0.3	$L_1/\lambda355/E21//D_1$
			Li I 670.78	2.5	$CO_2/666//L_1/\lambda1064/E100//D_3$
Leaves [260, 261]			Sn I 303.41	26	$CO_2/666//L_1/\lambda1064/E100//D_3$
B I 249.77	0.5	$Ar//L_1/\lambda1064/E365//D_1$	Sr II 407.77	1.2	$CO_2/666//L_1/\lambda1064/E100//D_3$
Ca I 422.67	80	$Ar//L_1/\lambda1064/E365//D_1$	N I 746.83	8000	$5//L_1/\lambda1064/E60//D_1$
Fe II 259.94	1.3	$Ar//L_1/\lambda1064/E365//D_1$	P I 178.28	280	$CO_2/709//L_1/\lambda1064/E40//D_1$
Mg I 277.98	30	$Ar//L_1/\lambda1064/E365//D_1$	Tl I 351.92	0.5	$L_1 + L_5/\lambda1064 + 276.78/E80 + 0.04/\Delta20/oc//D_2$
Mn II 257.61	0.5	$L_1/\lambda1064/E365//D_1$	Cd I 228.80	0.3	$L_1 + L_5/\lambda1064 + 228.80/E80 + 0.016/\Delta20/oc//D_2$
P I 214.91	20	$L_1/\lambda1064/E365//D_1$	Mg I 285.21	10	$L_1 + L_1/\lambda1064 + 532/E30 + 45/\Delta0.5/oc//D_1$
Cu I 324.75	2.5	$L_1/\lambda1064/E365//D_1$	Si I 288.16	600	$L_1 + L_1/\lambda1064 + 532/E30 + 45/\Delta0.5/oc//D_1$
Zn II 206.20	1	$L_1/\lambda1064/E365//D_1$			
			Coal [280 – 282]		
Mica [135, 262]			Si I 288.16	200	$L_1/\lambda1064/E38//D_1$
Li I 670.78	5	$L_1/\lambda266/E2.6//D_3$	S II 545.38	1000	$L_1 + L_1/\lambda1064 + 1064/E60 + 60/\Delta10/cc//D_4$
Na I 589	2700	$L_4/\lambda400/E4 \times 10^{-5}/\tau100//D_1$	Fe II 238.20	90	$L_1/\lambda1064/E38//D_1$
			Ca II 393.37	60	$L_1/\lambda1064/E90//D_4$
Ice [263]			Mg I 285.21	90	$L_1/\lambda1064/E90//D_4$
Na I 588.99	2	$L_2/\lambda10.6\ \mu m//D_1$	Na I 589	2700	$L_1/\lambda1064/E90//D_4$
Quartz [228]					
Na I 589.59	$4 \cdot 10^{-5}$	$MWP/100\ W//Ar/2 \times 10^4//L_1/\lambda1064/E30//D_3$			

Table 2 (continued).

Line	c_{min}	Conditions
Industrial oils, petroleum products [268, 269, 283, 284]		
Ca II 393.37	0.3	L//L_1/λ532/E60//D_1
Na I 588.99	0.7	L//L_1/λ532/E60//D_1
Pb I 405.78	90	L//L_1/λ532/E60//D_1
Sn I 284.00	80	L//L_1/λ532/E60//D_1
Pt I 306.47	90	Jet//N_2//L_1/λ266/E8//D_1
Cd II 226.50	4	L_1 + L_1/λ1064 + 1064/E95 + 170/Δ1/cc//D_1
Cr I 425.43	12	L_1 + L_1/λ1064 + 1064/E95 + 170/Δ1/cc//D_1
Cu I 324.75	1	L_1 + L_1/λ1064 + 1064/E95 + 170/Δ1/cc//D_1
Fe II 259.94	3	L_1 + L_1/λ1064 + 1064/E95 + 170/Δ1/cc//D_1
Mn II 257.61	3	L_1 + L_1/λ1064 + 1064/E95 + 170/Δ1/cc//D_1
Mo II 281.62	5	L_1 + L_1/λ1064 + 1064/E95 + 170/Δ1/cc//D_1
Ni I 339.30	7	L_1 + L_1/λ1064 + 1064/E95 + 170/Δ1/cc//D_1
Ti II 334.90	2	L_1 + L_1/λ1064 + 1064/E95 + 170/Δ1/cc//D_1
V II 310.23	2	L_1 + L_1/λ1064 + 1064/E95 + 170/Δ1/cc//D_1
Zn II 202.55	2	L_1 + L_1/λ1064 + 1064/E95 + 170/Δ1/cc//D_1
Mg II 279.55	0.4	Jet//L_1/λ1064/E150//D_1
Si I 251.61	11	Jet//L_1/λ1064/E150//D_1
Industry-produced waters [211, 270–273]		
B I 249.77	0.01	L_1/λ1064/E200//D_4
Cd I 228.80	8×10^{-4}	ED//L_1/λ1064/E50//D_2
Fe II 259.94	0.016	L_1 + L_1/λ532 + 532/E600 + 160/Δ1/cc//D_3
Cr I 425.43	39	L_1/λ1064/E200//D_4
Pb I 405.78	0.035	Jet//L_1 + L_5/λ266 + 283.31/E0.17 + 0.01/Δ0.3/oc//D_1
Natural waters [274, 275]		
Ca I 422.67	500	L/2.76 × 10^7//L_1 + L_1/λ1064 + 1064/E100 + 140/Δ0.05/cc//D_1
Mn I 403.07	1000	L/2.76 × 10^7//L_1 + L_1/λ1064 + 1064/E100 + 140/Δ0.05/cc//D_1
K I 769.89	500	L/2.76 × 10^7//L_1 + L_1/λ1064 + 1064/E100 + 140/Δ0.05/cc//D_1
Mg I 518.36	5000	L/2.76 × 10^7//L_1 + L_1/λ1064 + 1064/E100 + 140/Δ0.05/cc//D_1
Na I 588.99	50	L/2.76 × 10^7//L_1 + L_1/λ1064 + 1064/E100 + 140/Δ0.05/cc//D_1
Aqueous solutions [104, 194, 212, 276–279, 282–299]		
Pb I 405.78	24×10^{-5}	Jet//L_1 + L_6/λ1064 + 193/E60 + 60/Δ2.5/cc//D_1
Sm I 471.71	1.9	PC//L_1/λ1064/E200//D_1
Sn I 284.00	0.3	HG//Ar//L_1/λ532/E80//D_1
Tc I 429.70	25	L_1/λ1064/E30//D_3
Eu I 459.40	5	L//L_1/λ532/E5//D_1
Ga I 417.20	3	L_6/λ193/E150//D_2
Aqueous solutions [104, 194, 212, 276–279, 282–299]		
Ag I 328.08	0.43	Ex//L_1/λ1064/E80/D_1
Cu I 324.75	0.0095	Ex//L_1/λ1064/E80/D_1
Al I 396.15	0.19	L_4/λ800/E1/τ80//D_1
K I 766.49	0.006	L_4/λ800/E1/τ80//D_1
Au I 267.6	13.5	L_1 + L_1/λ266 + 1064/E32 + 200 /Δ2/cc//D_1
Ba II 455.39	0.007	Jet//L_6/λ193/E13//D_1
Ca I 422.67	0.003	Jet//L_6/λ193/E16//D_1
As I 193.76	0.7	HG//Ar + H_2//L_1/λ532/ E30//D_2
Sb I 259.81	0.2	HG//Ar + H_2//L_1/λ532/ E30//D_2
Se I 196.09	0.6	HG//Ar + H_2//L_1/λ532/ E30//D_2
Cr II 283.56	0.4	L//L_1/λ532/E60//D_1
Si I 288.16	25	L//L_1/λ532/E60//D_1
Cd I 228.80	0.9	Jet//Ar//L_1/λ532/E100//D_1
Ce II 439.17	18	Jet//Ar//L_1/λ532/E100//D_1
Gd II 364.62	3	Jet//Ar//L_1/λ532/E100//D_1
Mo I 386.40	2	Jet//Ar//L_1/λ532/E100//D_1
Nd II 430.36	10	Jet//Ar//L_1/λ532/E100//D_1
Pr II 440.88	3	Jet//Ar//L_1/λ532/E100//D_1
Sr II 421.54	0.39	Jet//Ar//L_1/λ532/E100//D_1
Y II 371.03	0.8	Jet//Ar//L_1/λ532/E100//D_1
Zr II 343.81	3	Jet//Ar//L_1/λ532/E100//D_1
Ge I 265.11	0.2	HG//Ar//L_1/λ532/E130//D_1
Hg I 253.65	0.002	ED + S/4kV/20A//L_1/λ1064/E10//D_2
In I 410.17	10	L//L_1 + L_1 + L_5/λ532 + 532 + 451.1/ F0.54 + 0.49 + 0.005/Δ100 + 1.2/cc//D_1
Li I 670.79	8×10^{-4}	Jet//L_1 + L_1/λ532 + 532/E30 + 100/Δ12/cc//D_1
Mg II 279.55	0.034	L//L_1/λ1064 + 1064/E72 + 144/Δ75/cc//D_1
Mn II 257.61	0.39	L//L_1/λ1064 + 1064/E72 + 144/Δ75/cc//D_1
Na I 588.99	1×10^{-4}	Jet//L_1 + L_1/λ1064 + 1064/E372/Δ8/oc//D_1
Ni I 352.45	0.06	AD//L_1/λ355/E14//D_1
Zn I 481.05	0.05	AD//L_1/λ355/E14//D_1
Th II 401.91	0.72	PC//L_1/λ1064/E200//D_4
U II 367.00	18.5	PC//L_1/λ1064/E200//D_4
Re I 346.05	8	Jet//L_1/λ532/E200//D_1
Fe I 373.49	0.065	L_1 + L_7/λ266 + 373.49/E40 + 0.01/Δ11/cc//D_1
Be II 313	10	L//L_1/λ1064/E42//D_2
Cs I 852.11	1	L//L_1/λ1064/E42//D_2
Rb I 780.03	0.2	L//L_1/λ1064/E42//D_2

copper. For other metals, for example, mercury, cadmium and thallium, LIBS analysis at the OEL level is still an open question. The same is true for some non-metals — arsenic, antimony and tellurium. It is also noteworthy that the development of a sensitive LIBS-based method for geochemical search for precious metals, rare earth and rare refractory metals (hafnium, tantalum, niobium) in soils, ores and rocks is still an unsolved problem. In the case of precious metals, the difficulty is due to their scattered occurrence as grains and, as a consequence, inhomogeneity of soils and ores. The detection of rare earth elements is hampered by fairly rich spectra and spectral interferences from Periodic Table neighbours. For liquid samples, the sensitivity is markedly higher and is generally comparable with the sensitivity of ICP – AES, the limits of detection being in the range of 0.01 – 10 mg litre^{-1}. In some cases it is possible to reach a sensitivity comparable with that of ICP – MS owing to the possibility of preconcentration, electrodeposition and extraction, for example, for some alkali metals, the limits of detection are tens or hundreds ppt.

V. Conclusion

The LIBS method is being actively developed and used more and more widely in the qualitative and quantitative analysis of natural samples, owing to its benefits — short time of analysis, the possibility to determine light and heavy elements in samples, the absence of sample preparation before measurements, the possibility of remote analysis and equipment reliability, which enables the design of portable and mobile devices. Currently, LIBS is successfully used to solve a number of important problems such as mapping of contamination of an area, identification of conflict minerals, environmental monitoring, analysis of natural objects that are difficult to access, for example, on sea bottom. LIBS is used for identification and quantitative analysis of natural objects on Mars due to the unique potential of this method. The wide scope of application of LIBS was the reason for inclusion of this method in educational programmes for students at different education levels. In this respect, not least important is relatively low cost of equipment to assemble an experimental bench in a student laboratory.[300 – 302]

The review describes the principles of LIBS, the key processes forming an analytical emission signal of the analyte elements and factors affecting this signal. It follows from the considered literature sources that the automated assignment of LIBS lines should take into account the variations of laser plasma parameters. The application of multivariate methods of data processing for qualitative and quantitative analysis is critically discussed for the first time. The use of multivariate models facilitates data interpretation; however, satisfactory results can now be obtained only for determining major and minor components in ores and soils. The multivariate models are useful for preliminary classification of samples in terms of the matrix composition, which allows one to choose samples for quantitative determination of traces of elements in natural objects with minimized matrix effects.

Analysis of the figures of merit reported in the literature demonstrated that the sensitivity of LIBS is sufficient for reliable and accurate determination of a number of elements (Pb, Zn, Be, Cu, Mo, *etc.*) at trace levels in soils and ores; this can be used for environmental monitoring and geochemical mapping. However, the problem of the sensitive determination of toxicants at OEL levels (Hg, Cd, Tl), precious metals, rare earth metals and rare refractory metals (Hf, Ta, Nb) in soils and rocks has not yet been solved.

The development of portable highly sensitive instruments would substantially extend the scope of application of LIBS. This can be expected in the near future. The progress in the production of miniature diode-pumped solid-state lasers can provide for a substantial decrease in the size of the source, while maintaining a high quality and power of the laser beam. The use of transmission gratings and hybrid systems combining diffraction and interference elements would serve to create a new generation of compact high-aperture instruments with good resolution over a broad spectral range. Commercial manufacture of new detectors based on CMOS technologies would allow the production of gated radiation detectors without expensive intensifiers.

This review was written with the financial support of the Russian Science Foundation (Project 14-13-01386).

References

1. D Cremers, L J Radziemski *Handbook of Laser-Induced Breakdown Spectroscopy* (Chichester: Wiley, 2006)
2. P Pease *Spectrochim. Acta, Part B* **83 – 84** 37 (2013)
3. X Zhu, T Xu, Q Lin, L Liang, G Niu, H Lai, M Xu, X Wang, H Li, Y Duan *Spectrochim. Acta, Part B* **93** 8 (2014)
4. J Frydenvang, K M Kinch, S Husted, M B Madsen *Anal. Chem.* **85** 1492 (2013)
5. M S Krzemnicki, H A Hanni, R A Walters *Gems Gemol.* **40** 314 (2004)
6. D C Alvey, K Morton, R S Harmon, J L Gottfried, J J Remus, L M Collins, M A Wise *Appl. Opt.* **49** C168 (2010)
7. C E McManus, N J McMillan, R S Harmon, R C Whitmore, F C De Lucia Jr, A W Miziolek *Appl. Opt.* **47** G72 (2008)
8. M Gaft, I Sapir-Sofer, H Modiano, R Stana *Spectrochim. Acta, Part B* **62** 1496 (2007)
9. L M Aksel'rod, V A Zaitsev, M B Sharov, A V Savchenko, A M Baryshnikov *Novye Ogneupory* **11** 21 (2012)
10. M Gaft, L Nagli, Y Groisman, A Barishnikov *Appl. Spectrosc.* **68** 1004 (2014)
11. M Gaft, L Nagli, N Eliezer, Y Groisman, O Forni *Spectrochim. Acta, Part B* **98** 39 (2014)
12. M Gaft, L Nagli, I Fasaki, M Kompitsas, G Wilsch *Spectrochim. Acta, Part B* **64** 39 (2009)
13. M V Bel'kov, V S Burakov, V V Kiris, V A Kononov, S N Raikov, V N Reshetnikov *J. Appl. Spectrosc.* **75** 275 (2008) [*Zh. Prikl. Spektrosk.* **75** 262 (2008)]
14. J Kwak, C Lenth, C Salb, E-J Ko, K-W Kim, K Park *Spectrochim. Acta, Part B* **64** 1105 (2009)
15. S Beldjilali, W L Yip, J Hermann, T Baba-Hamed, A Belasri *Anal. Bioanal. Chem.* **400** 2173 (2011)
16. D Derome, M Cathelineau, C Fabre, M C Boiron, D Banks, T Lhomme, M Cuney *Chem. Geol.* **237** 240 (2007)
17. N J McMillan, S Rees, K Kochelek, C McManus *Geostand. Geoanal. Res.* **38** 329 (2014)
18. B Thornton, T Sakka, T Takahashi, A Tamura, T Masamura, A Matsumoto *Appl. Phys. Expr.* **6** 082401 (2013)
19. B Thornton, T Sakka, T Masamura, A Tamura, T Takahashi, A Matsumoto *Spectrochim. Acta, Part B* **97** 7 (2014)
20. T Takahashi, B Thornton T Ura *Appl. Phys. Expr.* **6** 042403 (2013)
21. B Thornton, T Sakka, T Takahashi, A Tamura, A Matsumoto, T Ura, in *2013 IEEE International Underwater Technology Symposium (UT)* (New York: IEEE, 2013) p. 1

22. B Thornton, T Takahashi, T Sato, T Sakka, A Tamura, A Matsumoto, T Nozaki, T Ohki, K Ohki *Deep-Sea Research, Part I* **95** 20 (2015)
23. M Saeki, A Iwanade, C Ito, I Wakaida, B Thornton, T Sakka, H Ohba *J. Nucl. Sci. Technol.* **51** 930 (2014)
24. R Anderson, J C Bridges, A Williams, L Edgar, A Ollila, J Williams, M Nachon, N Mangold, M Fisk, J Schieber, S Gupta, G Dromart, R Wiens, S Le Mouélic, O Forni, N Lanza, A Mezzacappa, V Sautter, D Blaney, B Clark, S Clegg, O Gasnault, J Lasue, R Léveillé, E Lewin, K W Lewis, S Maurice, H Newsom, S P Schwenzer, D Vaniman *Icarus* **249** 2 (2015)
25. R C Wiens *Space Sci. Rev.* **170** 167 (2012)
26. J P Grotzinger *Science* **341** 1475 (2013)
27. P-J Meslin *Science* **341** 6153 (2013)
28. F Colao, R Fantoni, V Lazic, A Paolini, F Fabbri, G G Ori, L Marinangeli, A Baliva *Planet Space Sci.* **52** 117(2004)
29. B Sallé, J L Lacour, P Mauchien, P Fichet, S Maurice, G Manhès *Spectrochim. Acta, Part B* **61** 301 (2006)
30. *Laser-Induced Breakdown Spectroscopy: Fundamentals and Applications* (Eds A W Miziolek, V Palleschi, I Schechter) (Cambridge: Cambridge University Press, 2006)
31. *Laser-Induced Breakdown Spectroscopy* (Eds J P Singh, S N Thakur) (Amsterdam: Elsevier, 2007)
32. T A Labutin, V N Lednev, A M Popov, in *Laser-Induced Plasmas. Theory and Application* (Ed. E J Hemsworth) (New York: Nova, 2010) p. 145
33. R Noll *Laser-Induced Breakdown Spectroscopy: Fundamentals and Applications* (Berlin: Springer, 2012)
34. D A Cremers, L J Radziemski *Handbook of Laser-Induced Breakdown Spectroscopy* (2nd Ed.) (Chichester: Wiley, 2013)
35. K Song, Y-I Lee, J Sneddon *Appl. Spectrosc. Rev.* **37** 89 (2002)
36. E Tognoni, V Palleschi, M Corsi, G Cristoforetti *Spectrochim. Acta, Part B* **57** 1115 (2002)
37. A Giakoumaki, K Melessanaki, D Anglos *Anal. Bioanal. Chem.* **387** 749 (2007)
38. C Pasquini, J Cortez, L M C Silva, F B Gonzaga *J. Braz. Chem. Soc.* **18** 463 (2007)
39. R Fantoni, L Caneve, F Colao, L Fornarini, V Lazic, V Spizzichino *Spectrochim. Acta, Part B* **63** 1097 (2008)
40. D A Cremers, R C Chinni *Appl. Spectrosc. Rev.* **44** 457 (2009)
41. A M Popov, T A Labutin, N B Zorov *Moscow Univ. Chem. Bull.* **64** 366 (2009) [*Vestn. Mosk. un-ta. Ser. 2. Khimiya* **50** 453 (2009)]
42. F J Fortes, J J Laserna *Spectrochim. Acta, Part B* **65** 975 (2010)
43. R Gaudiuso, M Dell'Aglio, O De Pascale, G S Senesi, A De Giacomo *Sensors* **10** 7434 (2010)
44. D W Hahn, N Omenetto *Appl. Spectrosc.* **64** 335A (2010)
45. D W Hahn, N Omenetto *Appl. Spectrosc.* **66** 347 (2012)
46. A P M Michel *Spectrochim. Acta, Part B* **65** 185 (2010)
47. F J Fortes, J Moros, P Lucena, L M Cabalin, J J Laserna *Anal. Chem.* **85** 640 (2013)
48. R S Harmon, F C DeLucia, C E McManus, N J McMillan, T F Jenkins, M E Walsh, A W Miziolek *Appl. Geochem.* **21** 730 (2006)
49. R S Harmon, J Remus, N J McMillan, C McManus, L Collins, J L Gottfried Jr , F C DeLucia, A W Miziolek *Appl. Geochem.* **24** 1125 (2009)
50. R S Harmon, R E Russo, R R Hark *Spectrochim. Acta, Part B* **87** 11 (2013)
51. G S Senesi *Earth-Sci. Rev.* **139** 231 (2014)
52. S Qiao, Y Ding, D Tian, L Yao, G Yang *Appl. Spectrosc. Rev.* **50** 1 (2015)
53. L A Falkovsky, E G Mishchenko *J. Exp. Theor. Phys.* **88** 84 (1999) [*Zh. Eksp. Teor. Fiz.* **115** 149 (1999)]
54. S I Anisimov, B S Luk'yanchuk *Phys. Usp.,* **45** 293 (2002) [*Usp. Fiz. Nauk* **172** 301(2002)]
55. R E Russo, X Mao, J J Gonzalez, V Zorba, J Yoo *Anal. Chem.* **85** 6162 (2013)
56. D Autrique, G Clair, D L'Hermite, V Alexiades, A Bogaerts, B Rethfeld *J. Appl. Phys.* **114** 023301 (2013)
57. J M Fishburn, M J Withford, D W Coutts *Appl. Surf. Sci.* **252** 5182 (2006)
58. S N Andreev, S V Orlov, A A Samokhin *Phys. Wave Phenom.* **15** 67 (2007) [*Trudy IOFAN* **60** 127 (2004)]
59. S I Anisimov, B L Kapeliovich, T L Perelman *Sov. Phys. JETP* **39** (1974) 375 [*Zh. Eksp. Teor. Fiz.* **66** 776 (1974)]
60. S-S Wellershoff, J Hohlfeld, J Gmdde, E Matthias *Appl. Phys. A* **69** S99(1999)
61. V Margetic, A Pakulev, A Stockhaus, M Bolshov, K Niemax, R Hergenrlder *Spectrochim. Acta, Part B* **55** 1771 (2000)
62. X Zeng, X L Mao, R Greif, R E Russo *Appl. Phys. A* **80** 237 (2005)
63. G Seifert, M Kaempfe, F Syrowatka, C Harnagea, D Hesse, H Graener *Appl. Phys. A* **81** 799 (2005)
64. D Autrique, I Gornushkin, V Alexiades, Z Chen, A Bogaerts, B Rethfeld *Appl. Phys. Lett.* **103** 174102 (2013)
65. A Bogaerts, Z Chen *Spectrochim. Acta, Part B* **60** 1280 (2005)
66. A De Giacomo, M Dell'Aglio, R Gaudiuso, S Amoruso, O De Pascale *Spectrochim. Acta, Part B* **78** 1 (2012)
67. C Aragon, J A Aguilera *Spectrochim. Acta, Part B* **63** 893 (2008)
68. G W Rieger , M Taschuk, Y Y Tsui, R Fedosejevs *Spectrochim. Acta, Part B* **58** 497 (2003)
69. S Maurice, R C Wiens, M Saccoccio, M S L Team *Space Sci. Rev.* **170** 95 (2012)
70. J Cuñat, F J Fortes, L M Cabalín, F Carrasco, M D Simón, J J Laserna *Appl. Spectrosc.* **62** 1250 (2008)
71. J Rakovský, P Čermvk, O Musset, P Veis *Spectrochim. Acta, Part B* **101** 269 (2014)
72. M C Gupta, S T Peng *Appl. Opt.* **32** 2911 (1993)
73. H T Nguyen, B W Shore, S J Bryan, J A Britten, R D Boyd, M D Perry *Opt. Lett.* **22** 142 (1997)
74. A Weisberg, J Craparo, R De Saro, R Pawluczyk *Appl. Opt.* **49** C200 (2010)
75. Patent US 20130016349 (2013)
76. D Riebe, T Beitz, C Dosche, H-G Löhmannsröben, V Raab, C Raab, M Unverzagt *Appl. Spectrosc.* **68** 1030 (2014)
77. I B Gornushkin, B W Smith, U Panne, N Omenetto *Appl. Spectrosc.* **68** 1076 (2014)
78. M Sabsabi, R Héon, L St-Onge *Spectrochim. Acta, Part B* **60** 1211 (2005)
79. S M Zaytsev, A M Popov, N B Zorov, T A Labutin *J. Instrum.* **9** P06010 (2014)
80. T Sakka, K Irie, K Fukami, Y H Ogata *Rev. Sci. Instrum.* **82** 023112 (2011)
81. D Dussault, P Hoess *Proc. SPIE* **5563** 195 (2004)
82. Y Maruyama, J Blacksberg, E Charbon *IEEE J. Solid-State Circuits* **49** 179 (2014)
83. Q Lin, G Niu, Q Wang, Q Yu, Y Duan *Appl. Spectrosc. Rev.* **48** 487 (2013)
84. A Kramida, Y Ralchenko, J Reader *NIST Atomic Spectra Database (Ver. 5.2)* (Gaithersburg: National Institute of Standards and Technology, 2014)
85. R L Kurucz, B Bell *Kurucz's Atomic Line Database from CD-ROM* No. 23 (Cambridge: Smithsonian Astrophysical Observatory, 1995)
86. B Sharpee, R Williams, J A Baldwin, P A M van Hoof *Astrophys. J. (Suppl. Ser.)* **149** 157 (2003)
87. J Bengoechea, E T Kennedy *J. Anal. At. Spectrom.* **19** 468 (2004)
88. T Atwee, L Aschke, H-J Kunze *J. Phys. D* **33** 2263 (2000)
89. P Fichet, D Menut, R Brennetot, E Vors, A Rivoallan *Appl. Opt.* **42** 6029 (2003)
90. B Sallg, J-L Lacour, E Vors, P Fichet, S Maurice, D A Cremers, R C Wiens *Spectrochim. Acta, Part B* **59** 1413 (2004)

91. M P Mateo, G Nicolás, V Piñón, J C Alvarez, A Ramil, A Yáñez *Spectrochim. Acta, Part B* **60** 1202 (2005)
92. G Ukwatta, J Samarabandu, M Hall *Mach. Vis. Appl.* **23** 111 (2012)
93. G Amato, G Cristoforetti, S Legnaioli, G Lorenzetti, V Palleschi, F Sorrentino, E Tognoni *Spectrochim. Acta, Part B* **65** 664 (2010)
94. G Amato, G Cristoforetti, S Legnaioli, G Lorenzetti, V Palleschi, L Pardini, F Rabitti, in *Proceedings of the Fourth International Conference on Similarity Search and Applications (SISAP '11)* (New York: ACM, 2011) p. 89
95. B Miles, J Cortes *Field Anal. Chem. Technol.* **2** 75 (1998)
96. F Colao, R Fantoni, V Lazic, A Paolini *Appl. Phys., A* **79** 143 (2004)
97. R Fantoni, L Caneve, F Colao, L Fornarini, V Lazic, V Spizzichino, in *Advances in Spectroscopy for Lasers and Sensing* (Eds B Di Bartolo, O Forte) (Dordrecht: Springer, 2006) p. 229
98. W Hübert, G Ankerhold *Anal. Bioanal. Chem.* **400** 3273 (2011)
99. T A Labutin, S M Zaytsev, A M Popov *Anal. Chem.* **85** 1985 (2013)
100. S Zaytsev, A Popov, G Dzhedzheya, T Labutin, in *Boook of Absracts of 7th Euro-Mediterranean Symposium on Laser Induced Breakdown Spectroscopy, Bari, 2013* p. 208
101. T Trejos, Ph D Thesis Florida International Univercity, Miami, 2012
102. S Rock, A Marcano, Y Markushin, C Sabanayagam, N Melikechi *Appl. Opt.* **47** G99 (2008)
103. M D Dyar, J M Tucker, S Humphries, S M Clegg, R C Wiens, M D Lane *Spectrochim. Acta, Part B* **66** 39 (2011)
104. D Alamelu, A Sarkar, S K Aggarwal *Talanta* **77** 256 (2008)
105. A L Pomerantsev *Chemometrics in Excel*. Wiley 2014
106. P Geladi, B R Kowalski *Anal. Chim. Acta* **186** 1 (1986)
107. M M Tan, S Cui, J Yoo, S Han, K Ham, S Nam, Y Lee *Appl. Spectrosc.* **66** 262 (2012)
108. S C Jantzi, J R Almirall *Anal. Bioanal. Chem.* **400** 3341 (2011)
109. S M Clegg, E Sklute, M D Dyar, J E Barefield, R C Wiens *Spectrochim. Acta, Part B* **64** 79 (2009)
110. D L Death, A P Cunningham, L J Pollard *Spectrochim. Acta, Part B* **64** 1048 (2009)
111. P Pořízka, A Demidov, J Kaiser, J Keivanian, I Gornushkin, U Panne, J Riedel *Spectrochim. Acta, Part B* **101** 155 (2014)
112. J L Gottfried, R S Harmon, F C De Lucia Jr, A W Miziolek *Spectrochim. Acta, Part B* **64** 1009 (2009)
113. D C Alvey, K Morton, R S Harmon, J L Gottfried, J J Remus, L M Collins, M A Wise *Appl. Opt.* **49** C168 (2010)
114. R S Harmon, K M Shughrue, J J Remus, M A Wise, L J East, R R Hark *Anal. Bioanal. Chem.* **400** 3377 (2011)
115. R R Hark, J J Remus, L J East, R S Harmon, M A Wise, B M Tansi, K M Shughrue, K S Dunsin, C Liu *Spectrochim. Acta, Part B* **74 – 75** 131 (2012)
116. G Vítková, K Novotný, L Prokeš, A Hrdlička, J Kaiser, J Novotný, R Malina, D Prochazka *Spectrochim. Acta, Part B* **73** 1 (2012)
117. S Wold, M Sjöström, L Eriksson *Chemometr. Intell. Lab. Syst.* **58** 109 (2001)
118. S Wold *Technometrics* **20** 397 (1978)
119. D M Haaland, E V Thomas *Anal. Chem.* **60** 1193 (1988)
120. S M Zaytsev, A M Popov, E V Chernykh, R D Voronina, N B Zorov, T A Labutin *J. Anal. At. Spectrom.* **29** 1417 (2014)
121. J L Gottfried, F C De Lucia Jr, C A Munson, A W Miziolek *Spectrochim. Acta, Part B* **62** 1405 (2007)
122. I G Chong, C H Jun *Chemometr. Intell. Lab. Syst.* **78** 103 (2005)
123. O Forni, S Maurice, O Gasnault, R C Wiens, A Cousin, S M Clegg, J-B Sirven, J Lasue *Spectrochim. Acta, Part B* **86** 31 (2013)
124. A Hyvärinen, E Oja *Neural Networks* **13** 411 (2000)
125. A Koujelev, S-L Lui, in *Artificial Neural Networks — Industrial and Control Engineering Applications* (Ed. K Suzuki) (InTech, 2011) p. 91
126. S-L Lui, A Koujelev *J. Anal. At. Spectrom.* **26** 2419 (2011)
127. L Moenke-Blankenburg *Laser Microanalysis* (New York: Wiley, 1989)
128. J H Yoo, S H Jeong, R Greif, R E Russo *J. Appl. Phys.* **88** 1638 (2000)
129. M Guillong, I Horn, D Günther *J. Anal. At. Spectrom.* **17** 8 (2002)
130. Y Hirayama, H Yabe, M Obara *J. Appl. Phys.* **89** 2943 (2001)
131. Z D Cheng, M X Wen, W W Qiang, Z P Ju, Z X Long, L Bin, L H Ping *Chin. Phys. Lett.* **27** 063202 (2010)
132. J Gonzalez, X L Mao, J Roy, S S Mao, R E Russo *J. Anal. At. Spectrom.* **17** 1108 (2002)
133. J R Chirinos, D D Oropeza, J J Gonzalez, H Hou, M Morey, V Zorba, R E Russo *J. Anal. At. Spectrom.* **29** 1292 (2014)
134. V S Piscitelli, M A L Martínez, A J C Fernández, J J González, X L Mao, R E Russo *Spectrochim. Acta, Part B* **64** 147 (2009)
135. V Zorba, X Mao, R E Russo *Spectrochim. Acta, Part B* **66** 189 (2011)
136. S V Chekalin, V P Kandidov *Phys.-Usp.* **56** 123 (2013) [*Usp. Fiz. Nauk* **183** 133 (2013)]
137. K Stelmaszczyk, Ph Rohwetter, G Méjean, J Yu, E Salmon, J Kasparian, R Ackermann, J-P Wolf, L Wöste *Appl. Phys. Lett.* **85** 3977 (2004)
138. J-F Daiglea, P Mathieu, G Roy, J-R Simard, S L Chin *Opt. Commun.* **278** 147 (2007)
139. J Li, J Lu, Z Lin, S Gong, C Xie, L Chang, L Yang, P Li *Opt. Laser Technol.* **41** 907 (2009)
140. C Chaleard, P Mauchien, N Andre, J Uebbing, J L Lacour, C Geertsen *J. Anal. At. Spectrom.* **12** 183 (1997)
141. J Novotný, M Brada, M Petrilak, D Prochazka, K Novotný, A Hrdička, J Kaiser *Spectrochim. Acta, Part B* **101** 149 (2014)
142. B Sallé, D A Cremers, S Maurice, R C Wiens *Spectrochim. Acta, Part B* **60** 479 (2005)
143. H-R Kuhn, J Koch, R Hergenröder, K Niemax, M Kalberer, D Günther *J. Anal. At. Spectrom.* **20** 894 (2005)
144. H Lindner, J Koch, K Niemax *Anal. Chem.* **77** 7528 (2005)
145. V Kanicky, V Otruba, J-M Mermet *Fresenius J. Anal. Chem.* **363** 339 (1999)
146. C Liu, X L Mao, S S Mao, X Zeng, R Greif, R E Russo *Anal. Chem.* **76** 379 (2004)
147. W Gerlach, E Schweitzer *Die Chemische Emissions Spektralanalyse* Bd. 1 (Leipzig; LVoss, 1929)
148. N B Zorov, A A Gorbatenko, T A Labutin, A M Popov *Spectrochim. Acta, Part B* **65** 642 (2010)
149. J A M van der Mullen *Phys. Rep.* **191** 109 (1990)
150. W Demtröder *Atoms, Molecules and Photons. An Introduction to Atomic-, Molecular- and Quantum Physics* (Heidelberg: Springer 2010)
151. C Fabre, A Cousin, R C Wiens, A Ollila, O Gasnault, S Maurice, V Sautter, O Forni, J Lasue, R Tokar, D Vaniman, N Melikechi *Spectrochim. Acta, Part B* **99** 34 (2014)
152. Patent WO 97/15811 (1997)
153. U Panne, C Haisch, M Clara, R Niessner *Spectrochim. Acta, Part B* **53** 1957 (1998)
154. A S Eppler, D A Cremers, D D Hickmott, M J Ferris, A C Koskelo *Appl. Spectrosc.* **50** 1175 (1996)
155. T A Labutin, S M Zaytsev, A M Popov, I V Seliverstova, S E Bozhenko, N B Zorov *Spectrochim. Acta, Part B* **87** 57 (2013)
156. L Zhang, L Dong, H Dou, W Yin, S Jia *Appl. Spectrosc.* **62** 458 (2008)
157. P Yaroshchyk, J E Eberhardt *Spectrochim. Acta, Part B* **99** 138 (2014)

158. G Galbács, I Kevei-Bárány, E Szöke, N Jedlinszki, I B Gornushkin, M Z Galbács *Microchem. J.* **99** 406 (2011)
159. D M Díaz Pace, N A Gabriele, M Garcimuño, C A D'Angelo, G Bertuccelli, D Bertuccelli *Spectrosc. Lett.* **44** 399 (2011)
160. V Lazic, F Colao, R Fantoni, V Spizzichino *Spectrochim. Acta, Part B* **60** 1002 (2005)
161. V Lazic, F Colao, R Fantoni, V Spizzichino, S Jovièeviè *Spectrochim. Acta, Part B* **62** 30 (2007)
162. D W Hahn, W L Flower, K Henken *Appl. Spectrosc.* **51** 1836 (1997)
163. J E Carranza, D W Hahn *Spectrochim. Acta, Part B* **57** 779 (2002)
164. J E Carranza, K Lida, D W Hahn *Appl. Opt.* **42** 6022 (2003)
165. P Yaroshchyk, D L Death, S J Spencer *Appl. Spectrosc.* **64** 1335 (2010)
166. I B Gornushkin, P E Eagan, A B Novikov, B W Smith, J D Winefordner *Appl. Spectrosc.* **57** 197 (2003)
167. M D Dyar, M L Carmosino, J M Tucker, E A Brown, S M Clegg, R C Wiens, J E Barefield, J S Delaney, G M Ashley, S G Driese *Chem. Geol.* **294 – 295** 135 (2012)
168. R C Wiens, S Maurice, J Lasue, O Forni, R B Anderson, S Clegg, S Bender, D Blaney, B L Barraclough, A Cousin, L Deflores, D Delapp, M D Dyar, C Fabre, O Gasnault, N Lanza, J Mazoyer, N Melikechi, P-Y Meslin, H Newsom, A Ollila, R Perez, R L Tokar, D Vaniman *Spectrochim. Acta, Part B* **82** 1 (2013)
169. A M Ollila *J. Geophys. Res. Planets* **119** 255 (2014)
170. A M Popov, T A Labutin, S M Zaytsev, I V Seliverstova, N B Zorov, I A Kal'ko, Y N Sidorina, I A Bugaev, Y N Nikolaev *J. Anal. At. Spectrom.* **29** 1925 (2014)
171. A Ciucci, M Corsi, V Palleschi, S Rastelli, A Salvetti, E Tognoni *Appl. Spectrosc.* **53** 960 (1999)
172. E Tognoni, G Cristoforetti, S Legnaioli, V Palleschi *Spectrochim. Acta, Part B* **65** 1 (2010)
173. G Agrosü, G Tempesta, E Scandala, S Legnaioli, G Lorenzetti, S Pagnotta, V Palleschi, A Mangone, M Lezzerini *Spectrochim. Acta, Part B* **102** 48 (2014)
174. L Wang, C Zhang, Y Feng *Chin. Opt. Lett.* **6** 5 (2008)
175. A De Giacomo *Spectrochim. Acta, Part B* **66** 661 (2011)
176. M Dell'Aglio, A De Giacomo, R Gaudiuso, O De Pascale, S Longo *Spectrochim. Acta, Part B* **101** 68 (2014)
177. M Rossi, M Dell'Aglio, A De Giacomo, R Gaudiuso, G S Senesi, O De Pascale, F Capitelli, F Nestola, M R Ghiara *Phys. Chem. Miner.* **41** 127 (2014)
178. A De Giacomo, M Dell'Aglio, R Gaudiuso, A Santagata, G S Senesi, M Rossi, M R Ghiara, F Capitelli, O De Pascale *Chem. Phys.* **398** 233 (2012)
179. R L Rudnick, S Gao, in *Treatise on Geochemistry* Vol. 4 (2nd Ed.) (Ed. R L Rudnick) (Amsterdam: Elsevier, 2014) p. 1
180. K W Bruland, R Middag, M C Lohan, in *Treatise on Geochemistry* Vol. 8 (2nd Ed.) (Eds M J Mottl, H Elderfield) (Amsterdam: Elsevier, 2014) p. 19
181. *Official J. Eur. Commun.* L 181 4/7. Directive 86/27 6/EEC 1986
182. *Gigienicheskaya Otsenka Kachestva Pochvy Naselennykh Mest. Metodicheskie Ukazaniya MU 2.1.7.730-99* (Hygienic Assessment of Solid Quality in Residential Areas. Guidelines) (Moscow: Minzdrav RF 1999)
183. *Compendium of Analytical Nomenclature (Orange Book of IUPAC)* Definitive Rules 1997, Part 18.4.3.2
184. D M Templeton, F Ariese, R Cornelis, L-G Danielsson, H Muntau, H P van Leeuwen, R Lobinski *Pure Appl. Chem.* **72** 1453 (2000)
185. J E Sansonetti *J. Phys. Chem. Ref. Data* **37** 1659 (2008)
186. C Parigger *Spectrochim. Acta, Part B* **79 – 80** 4 (2013)
187. V S Burakov, N V Tarasenko, N A Savastenko *Spectrochim. Acta, Part B* **56** 961 (2001)
188. H Niki, T Yasuda, I Kitazima *J. Nucl. Sci. Technol.* **35** 34 (1998)
189. R E Russo, A A Bol'shakov, X Mao, C P McKay, D L Perry, O Sorkhabi *Spectrochim. Acta, Part B* **66** 99 (2011)
190. X Mao, A A Bol'shakov, D L Perry, O Sorkhabi, R E Russo *Spectrochim. Acta, Part B* **66** 604 (2011)
191. X Mao, A A Bol'shakov, I Choi, C P McKay, D L Perry, O Sorkhabi, R E Russo *Spectrochim. Acta, Part B* **66** 767 (2011)
192. M Dong, G C-Y Chan, X Mao, J J Gonzalez, J Lu, R E Russo *Spectrochim. Acta, Part B* **100** 62 (2014)
193. P S Doidge *Spectrochim. Acta, Part B* **50** 209 (1995)
194. D A Cremers, L J Radziemski, T R Loree *Appl. Spectrosc.* **38** 721 (1984)
195. A Y Bukharov, S M Pershin *J. Appl. Spectrosc.* **51** 1022 (1989) [*Zh. Prikl. Spektrosk.* **51** 564 (1989)]
196. K Y Yamamoto, D A Cremers, M J Ferris, L E Foster *Appl. Spectrosc.* **50** 222 (1996)
197. C Gautier, P Fichet, D Menut, J-L Lacour, D L Hermite, J Dubessy *Spectrochim. Acta, Part B* **59** 975 (2004)
198. E Tognoni, G Cristoforetti *J. Anal. At. Spectrom.* **29** 1318 (2014)
199. J Scaffidi, S M Angel, D A Cremers *Anal. Chem.* **78** 25 (2006)
200. A De Giacomo, M Dell'Aglio, O De Pascale, M Capitelli *Spectrochim. Acta, Part B* **62** 721 (2007)
201. V I Babushok, F C DeLucia Jr, J L Gottfried, C A Munson, A W Miziolek *Spectrochim. Acta, Part B* **61** 999 (2006)
202. H S Kwong, R M Measures *Anal. Chem.* **51** 428 (1979)
203. J D Winefordner, I B Gornushkin, D Pappas, O I Matveev, B W Smith *J. Anal. At. Spectrom.* **15** 1161 (2000)
204. P Stchur, K X Yang, X D Hou, T Sun, R G Michel *Spectrochim. Acta, Part B* **56** 1565 (2001)
205. D J Butcher *Appl. Spectrosc. Rev.* **42** 543 (2007)
206. H H Telle, D C S Beddows, G W Morris, O Samek *Spectrochim. Acta, Part B* **56** 947 (2001)
207. O N Ezhov, B R Kano, S V Oshemkov, A A Petrov *J. Appl. Spectrosc.* **56** 235 (1992) [*Zh. Prikl. Spektrosk.* **56** 394 (1992)]
208. I Gobernado-Mitre, A C Prieto, V Zafiropulos, Y Spetsidou, C Fotakis *Appl. Spectrosc.* **51** 1125 (1997)
209. F Hilbk-Kortenbruck, R Noll, P Wintjens, H Falk, C Becker *Spectrochim. Acta, Part B* **56** 933 (2001)
210. S Koch, W Garen, W Neu, R Reuter *Anal. Bioanal. Chem.* **385** 312 (2006)
211. S L Lui, Y Godwal, M T Taschuk, Y Y Tsui, R Fedosejevs *Anal. Chem.* **80** 1995 (2008)
212. H Loudyi, K Rifaï, S Laville, F Vidal, M Chaker, M Sabsabi *J. Anal At. Spectrom.* **24** 1421 (2009)
213. B W Smith, A Quentmeier, M Bolshov, K Niemax *Spectrochim. Acta, Part B* **54** 943 (1999)
214. A Quentmeier, M Bolshov, K Niemax *Spectrochim. Acta, Part B* **56** 45 (2001)
215. C A Smith, M A Martinez, D K Veirs, D A Cremers *Spectrochim. Acta, Part B* **57** 929 (2002)
216. D A Cremers, A Beddingfield, R Smithwick, R C Chinni, C R Jones, B Beardsley, L Karch *Appl. Spectrosc.* **66** 250 (2012)
217. S L Lui, N H Cheung *Anal. Chem.* **77** 2617 (2005)
218. K Rifai, F Vidal, M Chaker, M Sabsabi *J. Anal. At. Spectrom.* **28** 388 (2013)
219. F Brech, L Cross *Appl. Spectrosc.* **16** 59 (1962)
220. S D Rasberry, B F Scribner, M Margoshes *Appl. Opt.* **6** 87 (1967)
221. Patent RF 2163370 (2001)
222. O N Uskova, N V Pal'gunov, M Yu Razumovskaya, A Z Razyapov, A M Skrypkin *Ekolog. Sistem. Pribory* (4) 14 (2006)
223. M V Belkov, V S Burakov, A DeGiacomo, V V Kiris, S N Raikov, N V Tarasenko *Spectrochim. Acta, Part B* **64** 899 (2009)

224. K Li, W Zhou, Q Shen, Z Ren, B Peng *J. Anal. At. Spectrom.* **25** 1475 (2010)
225. K Li, W Zhou, Q Shen, J Shao, H Qian *Spectrochim. Acta, Part B* **65** 420 (2010)
226. Y Chen, Q Zhang, G Li, R Li, J Zhou *J. Anal. At. Spectrom.* **25** 1969 (2010)
227. J Uebbing, A Ciocan, K Niemax *Spectrochim. Acta, Part B* **47** 601 (1992)
228. A Ciocan, L Hiddemann, J Uebbing, K Niemax *J. Anal. At. Spectrom.* **8** 273 (1993)
229. Y Liu, M Baudelet, M Richardson *J. Anal. At. Spectrom.* **25** 1316 (2010)
230. Y Liu, B Bousquet, M Baudelet, M Richardson *Spectrochim. Acta, Part B* **73** 89 (2012)
231. M Tampo, M Miyabe, K Akaoka, M Oba, H Ohba, Y Maruyama, I Wakaida *J. Anal. At. Spectrom.* **29** 886 (2014)
232. D K Bhadra *Phys. Fluids* **11** 234 (1968)
233. V N Rai, H Zhang, F Y Yueh, J P Singh, A Kumar *Appl. Opt.* **42** 3662 (2003)
234. X K Shen, Y F Lu, T Gebre, H Ling, Y X Han *J. Appl. Phys.* **100** 053303 (2006)
235. M M Stoiljković, I A Pašti, M D Momčilović, J J Savović, M S Pavloviè *Spectrochim. Acta, Part B* **65** 927 (2010)
236. V N Rai, A K Rai, F Y Yueh, J P Singh *Appl. Opt.* **42** 2085 (2003)
237. A Neogi, R K Thareja *Appl. Phys., Part B* **72** 231 (2001)
238. A M Popov, F Colao, R Fantoni *J. Anal. At. Spectrom.* **24** 602 (2009)
239. A M Popov, F Colao, R Fantoni *J. Anal. At. Spectrom.* **25** 837 (2010)
240. L B Guo, C M Li, W Hu, Y S Zhou, B Y Zhang, Z X Cai, X Y Zeng, Y F Lu *Appl. Phys. Lett.* **98** 131501 (2011)
241. J-Z Chen, J-N Bai, G-J Song, J Sun, Z-C Deng, Y-L Wang *Appl. Opt.* **52** 6295 (2013)
242. C M Li, L Guo, X He, Z Hao, X G Li, M Shen, X Y Zeng, Y F Lu *J. Anal. At. Spectrom.* **29** 638 (2014)
243. X Su, W Zhou, H Qian *J. Anal. At. Spectrom.* **29** 2356 (2014)
244. Z Hao, L B Guo, C M Li, M Shen, X Zou, X G Li, Y F Lu, X Y Zeng *J. Anal. At. Spectrom.* **29** 2309 (2014)
245. Z Hou, Z Wang, J Liu, W Ni, Z Li *Opt. Expr.* **22** 12909 (2014)
246. Z Hou, Z Wang, J Liu, W Ni, Z Li *Opt. Expr.* **21** 15974 (2013)
247. *Compendium of Analytical Nomenclature (Orange Book of IUPAC)* Definitive Rules 1997, Part 10.2.1.1
248. R Payling, P Larkins *Optical Emission Lines of the Elements* (Chichester: Wiley, 2000)
249. A Uhl, K Loebe, L Kreuchwig *Spectrochim. Acta, Part B* **56** 795 (2001)
250. K J Grant, G L Paul, J A O'Neill *Appl. Spectrosc.* **45** 701 (1991)
251. C D Quarles Jr, J J Gonzalez, L J East, J H Yoo, M Morey, R E Russo *J. Anal. At. Spectrom.* **29** 1238 (2014)
252. Y Y Yoon, T S Kim, K S Chung, K Y Lee, G H Lee *Analyst* **122** 1223 (1997)
253. H Heilbrunner, N Huber, H Wolfmeir, E Arenholz, J D Pedarnig, J Heitz *Spectrochim. Acta, Part B* **74 – 75** 51 (2012)
254. Y S Kim, B Y Han, H S Shin, H D Kim, E C Jung, J H Jung, S H Na *Spectrochim. Acta, Part B* **74 – 75** 190 (2012)
255. I Rauschenbach, E K Jessberger, S G Pavlov, H-W Hübers *Spectrochim. Acta, Part B* **65** 758 (2010)
256. R A Multari, L E Foster, D A Cremers, M J Ferris *Appl. Spectrosc.* **50** 1483 (1996)
257. F Capitelli, F Colao, M R Provenzano, R Fantoni, G Brunetti, N Senesi *Geoderma* **106** 45 (2002)
258. G A Theriault, S Bodensteiner, S H Lieberman *Field Anal. Chem. Technol.* **2** 117 (1998)
259. A M Popov, M O Kozhnov, T A Labutin, S M Zaytsev, A N Drozdova, N A Mityurev *Tech. Phys. Lett.* **39** 81 (2013) [*Pis'ma Zh. Tekh. Fiz.* **39** 54 (2013)]
260. L C Nunes, J W B Braga, L C Trevizan, P F de Souza, G G A de Carvalho, D Santos Jr, R J Poppi, F J Krug *J. Anal. At. Spectrom.* **25** 1453 (2010)
261. L C Trevizan, D Santos Jr, R E Samad, N D Vieira Jr, L C Nunes, I A Rufini *Spectrochim. Acta, Part B* **64** 369 (2009)
262. C Fabre, M-C Boiron, J Dubessy, A Chabiron, B Charoy, T M Crespo *Geochim. Cosmochim. Acta* **66** 1401 (2002)
263. J O Cáceres, J T López, H H Telle, A G Ureña *Spectrochim. Acta Part B* **56** 831 (2001)
264. A K Knight, N L Scherbarth, D A Cremers, M J Ferris *Appl. Spectrosc.* **54** 331 (2000)
265. R D Harris, D A Cremers, M H Ebinger, B K Bluhm *Appl. Spectrosc.* **58** 770 (2004)
266. L Radziemski, D A Cremers, K Benelli, C Khoo, R D Harris *Spectrochim. Acta Part B* **60** 237 (2005)
267. T Čtvrtníčková, L M Cabalín, J Laserna, V Kanický *Spectrochim. Acta, Part B* **63** 42 (2008)
268. P Yaroshchyk, R J S Morrison, D Body, B L Chadwick *Spectrochim. Acta, Part B* **60** 1482 (2005)
269. P Yaroshchyk, R J S Morrison, D Body, B L Chadwick *Spectrochim. Acta, Part B* **60** 986 (2005)
270. A Sarkar, S K Aggarwal, K Sasibhusan, D Alamelu *Microchim. Acta* **168** 65 (2010)
271. F Zhao, Z Chen, F Zhang, R Li, J Zhou *Anal. Methods* **2** 408 (2010)
272. S Nakamura, Y Ito, K Sone, H Hiraga, K-i Kaneko *Anal. Chem.* **68** 2981 (1996)
273. M Y Yao, J L Lin, M H Liu, Y Xu *Appl. Opt.* **51** 1552 (2012)
274. A P M Michel, A D Chave *Appl. Opt.* **47** G122 (2008)
275. A P M Michel, A D Chave *Appl. Opt.* **47** G131 (2008)
276. N E Schmidt, S R Goode *Appl. Spectrosc.* **56** 370 (2002)
277. S S Golik, O A Bukin, A A Il'in, E B Sokolova, A V Kolesnikov, M Y Babiy, Y N Kul'chin, A A Gal'chenko *J. Appl. Spectrosc.* **79** 471 (2012) [*Zh. Prikl. Spektrosk.* **79** 488 (2012)]
278. K Rifai, S Laville, F Vidal, M Sabsabi, M Chaker *J. Anal. At. Spectrom.* **27** 276 (2012)
279. K M Lo, N H Cheung *Appl. Spectrosc.* **56** 682 (2002)
280. V S Burakov, N V Tarasenko, M I Nedelko, V A Kononov, N N Vasilev, S N Isakov *Spectrochim. Acta, Part B* **64** 141 (2009)
281. F J Wallis, B L Chadwick, R J S Morrison *Appl. Spectrosc.* **54** 1231 (2000)
282. D Body, B L Chadwick *Rev. Sci. Instrum.* **72** 1625 (2001)
283. P Fichet, P Mauchien, J-F Wagner, C Moulin *Anal. Chim. Acta* **429** 269 (2001)
284. F A Barreda, F Trichard, S Barbier, N Gilon, L Saint-Jalmes *Anal. Bioanal. Chem.* **403** 2601 (2012)
285. J B Simeonsson, L J Williamson *Spectrochim. Acta, Part B* **66** 754 (2011)
286. P Fichet, M Tabarant, B Salle, C Gautier *Anal. Bioanal. Chem.* **385** 338 (2006)
287. S U Yesiller, S Yalcin *Anal. Chim. Acta* **770** 7 (2013)
288. X Fang, S R Ahmad *Appl. Phys., Part B* **106** 453 (2012)
289. D-H Lee, S-C Han, T-H Kim, J-I Yun *Anal. Chem.* **83** 9456 (2011)
290. V Lazic, S Jovicevic, R Fantoni, F Colao *Spectrochim. Acta, Part B* **62** 1433 (2007)
291. A Kuwako, Y Uchida, K Maeda *Appl. Opt.* **30** 6052 (2003)
292. S T Jarvinen, S Saari, J Keskinen, J Toivonen *Spectrochim. Acta, Part B* **99** 9 (2014)
293. A Sarkar, D Alamelu, S K Aggarwal *Appl. Opt.* **47** G58 (2008)
294. F-Y Yueh, R C Sharma, J P Singh, H Zhang, W A Spencer *J. Air Waste Manage Assoc.* **52** 1307 (2002)

295. S Ünal, S Yalçin *Spectrochim. Acta, Part B* **65** 750 (2010)
296. O Samek, D C S Beddows, J Kaiser, S V Kukhlevsky, M Liška, H H Telle, J Young *Opt. Eng.* **39** 2248 (2000)
297. J-I Yun, T Bundschuh, V Neck, J-I Kim *Appl. Spectrosc.* **55** 273 (2001)
298. K C Ng, N L Ayala, J B Simeonsson, J D Winefordner *Anal. Chim. Acta* **269** 123 (1992)
299. S K Ho, N H Cheung *Anal. Chem.* **77** 193 (2005)
300. R C Chinni *J. Chem. Educ.* **89** 678 (2012)
301. M L Najarian, R C Chinni *J. Chem. Educ.* **90** 244 (2013)
302. D W Randall, R T Hayes, P A Wong *J. Chem. Educ.* **90** 456 (2013)